

The Dependence of Type Ia Supernova Luminosities on their Host Galaxies

M. Sullivan^{1*}, A. Conley², D. A. Howell^{3,4}, J. D. Neill⁵, P. Astier⁶, C. Balland^{7,8}, S. Basa⁸, R. G. Carlberg⁹, D. Fouchez¹⁰, J. Guy⁶, D. Hardin⁶, I. M. Hook^{1,11}, R. Pain⁶, N. Palanque-Delabrouille¹², K. M. Perrett^{9,13}, C. J. Pritchett¹⁴, N. Regnault⁶, J. Rich¹², V. Ruhlmann-Kleider¹², S. Baumont^{15,6}, E. Hsiao¹⁶, T. Kronborg⁶, C. Lidman¹⁷, S. Perlmutter^{18,16}, E. S. Walker^{19,1}

¹*Department of Physics (Astrophysics), University of Oxford, DWB, Keble Road, Oxford OX1 3RH, UK*

²*Department of Astrophysical and Planetary Sciences, University of Colorado, Boulder, CO 80309-0391, USA*

³*Las Cumbres Observatory Global Telescope Network, 6740 Cortona Dr., Suite 102, Goleta, CA 93117, USA*

⁴*Department of Physics, University of California, Santa Barbara, Broida Hall, Mail Code 9530, Santa Barbara, CA 93106-9530, USA*

⁵*California Institute of Technology, 1200 E. California Blvd., Pasadena, CA 91125, USA*

⁶*LPNHE, Université Pierre et Marie Curie Paris 6, Université Paris Diderot Paris 7, CNRS-IN2P3, 4 place Jussieu, 75252 Paris Cedex 05, France.*

⁷*University Paris 11, Orsay, F-91405, France*

⁸*LAM, Pole de l'Etoile Site de Chateau-Gombert, 38 rue Frederic Joliot-Curie, 13388 Marseille Cedex 13, France*

⁹*Department of Astronomy and Astrophysics, University of Toronto, 50 St. George Street, Toronto ON M5S 3H4, Canada*

¹⁰*CPPM, Aix-Marseille Université, CNRS/IN2P3, 13288 Marseille Cedex 9, France*

¹¹*INAF - Osservatorio Astronomico di Roma, via Frascati 33, 00040 Monteporzio (RM), Italy*

¹²*CEA/Saclay, DSM/Irfu/Spp, 91191 Gif-sur-Yvette Cedex, France*

¹³*Network Information Operations, DRDC Ottawa, 3701 Carling Avenue, Ottawa, ON, K1A 0Z4, Canada*

¹⁴*Department of Physics and Astronomy, University of Victoria, P.O. Box 3055 STN CSC, Victoria BC V8T 1M8, Canada*

¹⁵*LPSC, CNRS-IN2P3, 53 rue des Martyrs, 38026 Grenoble Cedex, France*

¹⁶*Lawrence Berkeley National Laboratory, Mail Stop 50-232, Lawrence Berkeley National Laboratory, 1 Cyclotron Road, Berkeley, CA 94720, USA*

¹⁷*Anglo-Australian Observatory, P.O. Box 296, Epping, NSW 1710, Australia*

¹⁸*Department of Physics, University of California, 366 LeConte Hall MC 7300, Berkeley, CA 94720-7300, USA*

¹⁹*Scuola Normale Superiore, Piazza dei Cavalieri 7, 56126 Pisa, Italy*

24 October 2018

arXiv:1003.5119v1 [astro-ph.CO] 26 Mar 2010

ABSTRACT

Precision cosmology with Type Ia supernovae (SNe Ia) makes use of the fact that SN Ia luminosities depend on their light-curve shapes and colours. Using Supernova Legacy Survey (SNLS) and other data, we show that there is an additional dependence on the global characteristics of their host galaxies: events of the same light-curve shape and colour are, on average, 0.08 mag ($\simeq 4.0\sigma$) brighter in massive host galaxies (presumably metal-rich) and galaxies with low specific star-formation rates (sSFR). These trends do not depend on any assumed cosmological model, and are independent of the SN light-curve width: both fast and slow-declining events show the same trends. SNe Ia in galaxies with a low sSFR also have a smaller slope (“ β ”) between their luminosities and colours with $\sim 2.7\sigma$ significance, and a smaller scatter on SN Ia Hubble diagrams (at 95% confidence), though the significance of these effects is dependent on the reddest SNe. SN Ia colours are similar between low-mass and high-mass hosts, leading us to interpret their luminosity differences as an intrinsic property of the SNe and not of some external factor such as dust. If the host stellar mass is interpreted as a metallicity indicator using galaxy mass–metallicity relations, the luminosity trends are in qualitative agreement with theoretical predictions. We show that the average stellar mass, and therefore the average metallicity, of our SN Ia host galaxies decreases with redshift. The SN Ia luminosity differences consequently introduce a systematic error in cosmological analyses, comparable to the current statistical uncertainties on parameters such as w , the equation of state of dark energy. We show that the use of two SN Ia absolute magnitudes, one for events in high-mass (metal-rich) galaxies, and one for events in low-mass (metal-poor) galaxies, adequately corrects for the differences. Cosmological fits incorporating these terms give a significant reduction in χ^2 (3.8–4.5 σ); linear corrections based on host parameters do not perform as well. We conclude that all future SN Ia cosmological analyses should use a correction of this (or similar) form to control demographic shifts in the underlying galaxy population.

Key words: supernovae: general – cosmology: observations – distance scale.

1 INTRODUCTION

As calibrateable standard candles, Type Ia supernovae (SNe Ia) provide a direct route to understanding the nature of the dark energy that drives the accelerated expansion of the Universe. Yet, the relationships that allow the calibration of their peak luminosities, and hence permit their cosmological use, remain purely empirical. Relations between the width of the SN Ia light curve and peak luminosity (Phillips 1993) and between the SN Ia optical colours and luminosity (e.g. Riess et al. 1996; Tripp 1998) reduce the scatter in their peak magnitudes to ~ 0.15 mag (Jha et al. 2007; Guy et al. 2007; Conley et al. 2008). As the available SN Ia samples increase in both size and quality, and the dark energy constraints they provide become correspondingly more statistically precise, it is increasingly important that the validity of these calibrating relationships is robustly examined.

The observed properties of SNe Ia are known to correlate with the physical parameters defining their host galaxy stellar populations. SNe Ia are more than an order of magnitude more common (per unit stellar mass) in actively star-forming or morphologically late-type galaxies than in passive or elliptical systems (Mannucci et al. 2005; Sullivan et al. 2006). SNe Ia in elliptical or passively evolving systems are also intrinsically fainter, with narrower, faster (or lower “stretch”), light curves (Hamuy et al. 1995,

1996b; Riess et al. 1999; Hamuy et al. 2000; Sullivan et al. 2006). Though this effect is corrected for by the light-curve shape correction, the amount of star formation activity in the universe increases with redshift, and these differences lead to an observed “demographic shift” in mean SN Ia properties. A greater fraction of intrinsically luminous, wider light-curve events in the distant universe are seen compared to that observed locally (Howell et al. 2007). These photometric differences are also partially reflected in SN Ia spectra, with SNe Ia in spiral galaxies showing weaker intermediate mass element line strengths than those in elliptical galaxies (Bronder et al. 2008; Balland et al. 2009), and a corresponding evolution in the mean SN Ia spectrum with redshift (Sullivan et al. 2009).

There are suggestions that these effects may be the result of multiple astrophysical channels capable of producing SN Ia explosions (e.g. Scannapieco & Bildsten 2005; Mannucci et al. 2006). In particular, delay-time distributions with distinct “prompt” and “delayed” components, or with a wide range of delay-times, match most observational datasets well (Mannucci et al. 2006; Sullivan et al. 2006; Pritchett et al. 2008; Totani et al. 2008), though the minimum age for the prompt systems remains controversial (Aubourg et al. 2008; Raskin et al. 2009) with some evidence that “prompt” SNe Ia occur more frequently in metal-poor systems (Cooper et al. 2009). The use of SNe Ia as precision cosmological probes therefore depends on establishing that the demographic shifts, or existence of

* E-mail: sullivan@astro.ox.ac.uk

multiple channels to a SN Ia, do not impact on the light-curve-width/colour/luminosity relationships. If these relationships show environmental dependence, then the task of calibrating SNe Ia for cosmology becomes substantially more challenging (e.g. Sarkar et al. 2008; Kelly et al. 2009).

A second complication arises from the (poorly understood) colour corrections applied to SN Ia luminosities. Redder SNe Ia appear fainter than their bluer counterparts, but the slope of the relationship between SN Ia colour and magnitude is inconsistent with the ratio of total-to-selective absorption appropriate for the diffuse interstellar medium of the Milky Way ($R_V = 3.1$). Multiple studies of different SN Ia samples indicate that the effective R_V inferred from normal SNe Ia is smaller than 3.1 (e.g., Tripp 1998; Astier et al. 2006; Krisciunas et al. 2006), and the *assumption* of $R_V = 3.1$, even after light curve shape corrections, leads to serious systematic error problems such as a spurious ‘‘Hubble Bubble’’ (Jha et al. 2007; Conley et al. 2007). The reason for this low effective R_V is not well understood. Although uncorrected intrinsic variations in the SN Ia population could play a role (e.g. Kasen et al. 2009), some dust extinction must also affect the SN Ia luminosities and colours, and this may vary by environment. Furthermore, the exact value of R_V obtained is sensitive to method used to determine it, with lower R_V obtained when fitting linear relations between SN Ia luminosities, colours, and light curve widths (Folatelli et al. 2010), perhaps due to intrinsic variation in SN Ia colours that correlates with luminosity but not light-curve width. Current knowledge of SNe Ia is not sufficient to separate and correct for both intrinsic colour–luminosity and dust-induced colour–luminosity effects in cosmological SN Ia samples.

Examining how SN Ia luminosities vary with environment after light curve shape and colour corrections can place constraints on the degree of these possible variations. Early studies showed little evidence that corrected SN Ia luminosities varied with host galaxy morphologies (e.g., Perlmutter et al. 1999; Riess et al. 1999; Sullivan et al. 2003; Williams et al. 2003; Gallagher et al. 2005), though these tests used relatively small samples of events ($\lesssim 50$), in some cases from the first-generation of SN Ia cosmological samples before dense multi-colour light curves were routinely obtained.

More recent analyses, using larger, well-observed samples, have shown tentative evidence for variation. Hicken et al. (2009b) found $\simeq 2\sigma$ evidence that SNe Ia in morphologically E/S0 galaxies are brighter than those in later-type spirals after light-curve shape and colour corrections. Extending beyond simple host galaxy morphologies to more physically motivated variables gives further tantalising suggestions of variation. Gallagher et al. (2008) found evidence for a correlation between Hubble diagram residual and host galaxy stellar metallicity in a sample of 17 local SNe Ia located in E/S0 galaxies, in the sense that fainter SNe Ia after correction were found in metal poor systems (note this is the reverse of the originally published trend due to an error in the original analysis; P. Garnavich, private communication). Howell et al. (2009) used 55 SNe Ia from the first year of the SNLS and showed no significant correlation between Hubble residual and host galaxy metallicity, albeit using host gas-phase metallicities inferred from average galaxy stellar-mass–metallicity relations, a less direct

measure of metallicity. Kelly et al. (2009) have shown a relation between host galaxy stellar mass and Hubble residual, in the sense that more massive systems host brighter SNe Ia after light curve shape and colour corrections. Under the assumption that more massive galaxies are metal rich, this trend is consistent with the revised Gallagher et al. (2008) result.

In this paper, we use a sample of 282 high redshift SNe Ia discovered and photometrically monitored by the Canada-France-Hawaii Telescope (CFHT) as part of the Supernova Legacy Survey (SNLS), and which form the SNLS ‘‘three-year’’ sample (SNLS3). Using deep optical imaging of their host galaxies taken over the duration of the survey, we place constraints on their recent star-formation activity, stellar masses (and hence inferred metallicity), and compare to the photometric properties of the SNe Ia that they host. In particular, we search for evidence that the corrected SN Ia luminosities correlate with these host properties, indicating possible systematic errors in the light curve fitting framework that underpins their cosmological use. We compare with the properties of a sample of lower-redshift SNe Ia taken from the literature.

A plan of the paper follows. In § 2 we introduce the SN Ia sample and the data available on their host galaxies. § 3 investigates how the SN Ia light curve widths and colours of these SNe Ia varies according to their host galaxy properties, and in § 4 we compare their corrected luminosities to the host properties. We discuss the results, including the cosmological implications, in § 5, and conclude in § 6. Throughout, where relevant we assume a flat Λ CDM cosmological model with $\Omega_M = 0.256$ (the reason for this non-standard choice is explained in § 4) and $H_0 = 70 \text{ km s}^{-1} \text{ Mpc}^{-1}$ assumed in all quoted absolute magnitudes. All magnitudes are given on the Landolt (1992) photometric system as described in Regnault et al. (2009).

2 TYPE IA SUPERNOVA AND HOST GALAXY DATA

We begin by introducing the SN Ia samples that we will use in this paper, and the associated data available for their host galaxies.

2.1 The SN Ia samples

The high-redshift SN Ia data is taken from the Supernova Legacy Survey (SNLS). This used optical imaging data taken as part of the deep component of the five-year Canada-France-Hawaii Telescope Legacy Survey (CFHT-LS) using the square-degree ‘‘MegaCam’’ camera (Boulade et al. 2003), located in the prime focus environment ‘‘MegaPrime’’ on the CFHT. The ‘‘deep’’ component of CFHT-LS conducted repeat imaging of 4 low Galactic-extinction fields, time-sequenced with observations conducted every 3–4 nights in dark and grey time. Four filters, $g_{MR}m_{iM}z_M$, were used allowing the construction of high-quality multi-colour SN light curves; u_M data were also taken but are not time-sequenced. On each night of observations, the data were searched using two independent pipelines, and an amal-

gamated candidate list produced¹ (see Perrett et al. 2010). Spectroscopic follow-up confirmed SN types and measured redshifts to allow SNe Ia to be placed on a Hubble diagram.

In this paper we use SNe Ia belonging to the three-year sample, SNLS3; this includes all SNe Ia discovered up until the end of July 2006. The light curves and other details for these SNe can be found in Guy et al. (2010), and spectroscopic information is taken from Howell et al. (2005), Bronder et al. (2008), Ellis et al. (2008), Balland et al. (2009), and Walker et al. (2010). The full SNLS3 sample consists of 282 SNe Ia, however we exclude some of these events from some of our analyses:

(i) Only SNLS SNe Ia with an identified (§ 2.3) host galaxy (272 events) are considered (for a discussion of the identification procedures, see Sullivan et al. 2006, hereafter S06),

(ii) Only SNe Ia passing light curve quality cuts (e.g. Conley et al. 2008; Guy et al. 2010) are used – there must be sufficient photometric coverage to derive reliable peak luminosities, light curve widths, and colours (see details in Guy et al. 2010),

(iii) We only consider normal SNe Ia with light-curve parameters in the range considered for cosmological fits – our motivation in this paper is to assess the cosmological impact of any host galaxy dependent trends. Specifically, we require that the stretch of the SN be greater than 0.80, and that the colour be less than 0.30 (see § 2.2 for a discussion of the meaning of these parameters). We also discard $> 3\sigma$ outliers from the best fitting cosmological model. 231 events pass the light-curve coverage and SN parameter cuts.

(iv) In analyses where we search for trends in the SNLS data, we use only SNe Ia at redshift $z \leq 0.85$ (195 events). At these lower redshifts, both the SN and host galaxy photometry are higher signal-to-noise and their photometric parameters better measured. The SNLS Malmquist biases are also smaller (Perrett et al. 2010).

Where relevant, we also use samples of SNe Ia from the literature. We construct a sample of low-redshift SNe Ia from the compilation of Conley et al. (2010), which includes SNe Ia from a variety of sources (primarily Hamuy et al. 1996a; Riess et al. 1999; Jha et al. 2006; Hicken et al. 2009a; Contreras et al. 2009). We apply bulk-flow peculiar velocity corrections to the SN magnitudes and redshifts, placing the redshifts in the CMB-frame (z_{cmb}) following Neill et al. (2007), but with updated models (Conley et al. 2010). The accuracy of these corrections is estimated to $\pm 150 \text{ km s}^{-1}$, which we propagate into the SN magnitude errors in cosmological fits. We only use SNe Ia in the smooth Hubble flow, here defined as $z_{\text{cmb}} \geq 0.01$, and apply the same light curve quality cuts as for the SNLS sample. There are 110 low-redshift objects in total. We also use the *HST*-discovered sample of Riess et al. (2004) and Riess et al. (2007), hereafter the R07 sample. We select 24 SNe Ia at $z > 0.9$ from this sample to increase our redshift lever arm above $z = 1$.

2.2 SN Light curve fitting

In its current application, SN Ia cosmology depends on two corrections to “raw” SN Ia peak luminosities that when applied reduce the dispersion in their peak magnitudes. The first is the light-curve-shape/luminosity relation (e.g. Phillips 1993): brighter SNe Ia tend to have wider, longer-duration light curves (higher stretch) than their fainter counterparts. The second is a colour correction: brighter SNe Ia tend to have bluer colours, whilst fainter SNe tend to be redder (Riess et al. 1996; Tripp 1998). Together the application of these corrections can yield distance estimates precise to $\simeq 6$ per cent. These corrections are applied in different ways depending on whether a technique is a distance estimator (e.g., MLCS2k2; Jha et al. 2007) or a light curve fitter (e.g. SALT or SiFTO; Guy et al. 2007; Conley et al. 2008), though the underlying principle is the same in both approaches.

In this paper, we primarily use the SiFTO light curve fitter (Conley et al. 2008) and compare our results to SALT2 (Guy et al. 2007) where appropriate. In general SALT2 and SiFTO give very similar results when trained on the same SN sample – a full discussion can be found in Guy et al. (2010). Both fitters have been retrained and improved since the original published versions using SNLS and low-redshift data. The product of both fitters for each SN is a rest-frame *B*-band apparent magnitude (m_B), a stretch (s) measurement, and a colour estimate (C), together with associated errors and covariances (SALT2 uses the broadly equivalent x_1 parameter in place of s). Throughout, the SN Ia colour, C , is defined as the rest-frame ($B - V$) colour of the SN at the time of maximum light in the rest-frame *B*-band. We refit all SNe Ia using these light curve fitters to ensure that the different samples can be placed on the same distance scale. A full discussion of their application to the current dataset, together with their tabulated output, can be found in Guy et al. (2010) and Conley et al. (2010).

2.3 SN host galaxy photometry

Our SNLS host galaxy photometry comes in the optical from the CFHT-LS ($u_M g_M r_M i_M z_M$) and in the near infra red (IR) from the WIRcam Deep Survey (WIRDS; Bielby et al. in prep.) of a sub-section of the CFHT-LS fields (J, H, K_s). The identification procedure for the SNLS SN Ia host galaxies is the same as that in S06. Photometry is performed by SExtractor (Bertin & Arnouts 1996) using FLUX-AUTO photometry running in dual-image mode, detecting from the deep i_M stack and measuring from each of the optical and near-IR filters in turn (60% of our SN Ia hosts have near-IR data). Each stack has a similar image quality and hence the same physical aperture is used in each filter. In about $\simeq 3\%$ of cases no host galaxy can be identified. This could be because the SN lies far from the centre of its host galaxy leading to ambiguity in the correct choice of host, or because the host lies below the CFHT-LS flux limits. We discard these objects. Weight maps are used to determine the measurement errors, and in the optical, the photometric zeropoints are generated using a comparison to the tertiary standard star lists of Regnault et al. (2009). No SN light is present in the optical stacks which are constructed on a per season basis (S06).

¹ Candidates can be found at <http://legacy.astro.utoronto.ca/>

For the low-redshift sample, we use host galaxy photometry recently compiled by Neill et al. (2009, hereafter N09), including ultraviolet data from the GALEX (Galaxy Evolution Explorer) satellite, and optical photometry from the third reference catalog of bright galaxies (RC3; Corwin et al. 1994) and the Sloan Digital Sky Survey (SDSS). The photometry for this sample was carefully performed in matched apertures with foreground contaminating stars masked. Though these data span a different observed wavelength range compared to the SNLS host photometry, in the rest-frame the wavelength range covered is reasonably similar: the maximal range is 1500–9000Å for the low-redshift sample (though frequently the available data span a smaller range than this), and 2400–13000Å for the SNLS sample (at $z = 0.6$). Note that not all the low-redshift SN hosts have publicly available host photometry: only 69 (of 110; 63%) low-redshift SNe Ia have sufficient data and are carried forward in the analysis. The missing low-redshift SNe Ia are due to incomplete GALEX and SDSS coverage, rather than the host galaxies being too faint to be detected by the two surveys.

For the R07 sample, we use photometry taken from the Great Observatories Origins Deep Survey (GOODS) *HST* data (Giavalisco et al. 2004), taken with the Advanced Camera for Surveys (ACS). Data are available in four filters: F435W (broadly equivalent to a B filter), F606W (V), F814W (i') and F850LP (z'). All of the R07 SNe have ACS coverage, and again `SExtractor` FLUX_AUTO photometry is used. We also use J , H and K imaging taken as part of the GOODS NICMOS survey (e.g. Buitrago et al. 2008), as well as ground-based data (Retzlaff et al. 2009).

2.4 Host galaxy parameter estimation

The method to estimate physical parameters of the SN Ia host galaxies is similar to that in S06 which used the photometric redshift code Z-PEG (Le Borgne & Rocca-Volmerange 2002) based upon the PÉGASE.2 spectral synthesis code (e.g., Fioc & Rocca-Volmerange 1997). We use an expanded set of 15 exponentially declining star formation histories (SFHs) with $\text{SFR} \propto \exp^{-t/\tau}$, where t is time and τ is the e-folding time, each with 125 age steps. The internal PÉGASE.2 dust prescriptions are not used, and instead a foreground dust screen varying from $E(B - V) = 0$ to 0.30 in steps of 0.05 is added. With the 7 different foreground dust screens, this gives a total of 105 unique evolving spectral energy distributions (SEDs). The metallicity of the stellar population evolves consistently following the standard PÉGASE.2 model with an initial value of 0.0004, and the standard PÉGASE.2 nebular emission prescription is added.

Z-PEG is used to locate the best-fitting SED model (in a χ^2 sense), with the redshift fixed at the CMB-frame redshift of the SN. Only solutions younger than the age of the Universe at each SN redshift are permitted. The current stellar mass in stars (M_{stellar} , measured in M_{\odot}), the recent star formation rate (SFR, in $M_{\odot}\text{yr}^{-1}$, averaged over the last 0.25Gyr before the best fitting time step), and the specific star formation rate (sSFR, the SFR per unit stellar mass with units of yr^{-1} , e.g. Guzman et al. 1997) are all recorded. Error bars on these parameters are taken from their range in

the set of solutions that have a similar χ^2 (as in S06). Note that we do not measure the instantaneous SFR as we only fit broad-band photometry. We refit all the N09 photometry to ensure the exact same library SEDs are used for all hosts.

We use a Rana & Basu (1992) initial mass function (IMF), the PÉGASE.2 default, throughout. Our results are not sensitive to this choice – we have repeated our analysis in full with both the more standard Salpeter (1955) IMF, and with a Baldry & Glazebrook (2003) IMF, and find similar results, though the M_{stellar} and SFRs derived for the host galaxies have (expected) small mean offsets when using different IMFs. In detail, the use of a Salpeter IMF gives systematically larger host masses by 0.04 dex (smaller masses by 0.16 dex for the B&G IMF), and smaller SFRs by 0.04 dex (smaller by 0.16 dex for B&G), with scatter of around 0.1dex in each comparison. These differences are not a function of M_{stellar} , SFR or redshift and so have a negligible impact on our conclusions.

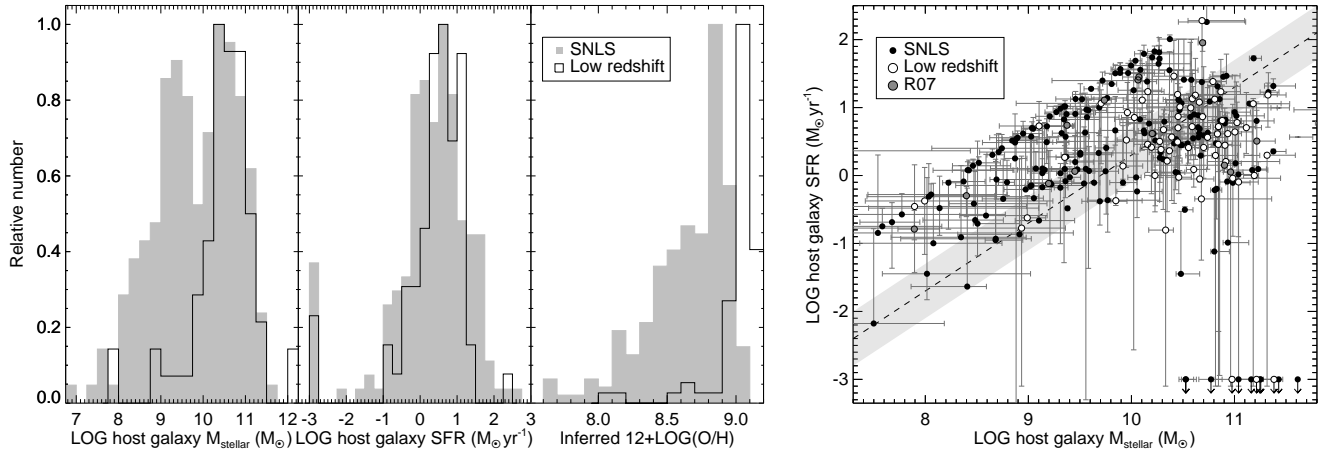
As only $\simeq 60\%$ of our SNLS SN Ia hosts have observer-frame near-IR data, we compare the derived properties with and without these data to check for potential biases in the remaining 40% of objects. The mean difference in M_{stellar} (defined as $M_{\text{stellar}}^{\text{OPT}} - M_{\text{stellar}}^{\text{IR}}$) is 0.001 dex (r.m.s. 0.15) and in the recent SFR the mean difference ($\text{SFR}^{\text{OPT}} - \text{SFR}^{\text{IR}}$) is -0.18 dex (r.m.s. 0.44), in the sense that excluding the IR data leads to smaller SFRs. Thus we find no evidence that the near-IR data leads to systematically different M_{stellar} , and mild evidence that including these data leads to larger SFRs. The differences in SFR do not follow a Gaussian distribution; instead the difference is centred around zero but with a long tail to negative differences; therefore we choose not to apply the mean offset to the 40% of hosts with no IR data. There is no evidence for any redshift dependent trend. Information on the derived properties for the SNLS, low-redshift and R07 hosts can be found in Table 1.

The M_{stellar} and SFR distributions for the SNLS and low-redshift samples are shown in Fig. 1, together with the distribution of galaxies in the $\text{SFR} - M_{\text{stellar}}$ plane. As might be expected, galaxies with the smallest sSFRs tend to be the most massive systems, with the lowest mass systems universally consistent with strong star formation activity. As previously highlighted by N09, the SNLS and low-redshift hosts show quite different distributions in M_{stellar} (and to a lesser extent SFR): The low-redshift SNe are drawn from more massive host galaxies. This is almost certainly due to selection biases. SNLS is a rolling search which will locate SNe Ia in any type of host galaxy in which they explode, and, modulo any small spectroscopic follow-up bias, this range will be reflected in the cosmological sample. At low-redshift, most SNe Ia are drawn from galaxy-targeted searches which search known (and typically bright/massive) galaxies, consequently the most massive systems will be over-represented.

Following Howell et al. (2009), we convert the M_{stellar} mass estimates into metallicities using average $M_{\text{stellar}} - \text{metallicity}$ ($M_{\text{stellar}} - Z$) relations. As the universe ages, galaxies will become more massive via merging processes, and more metal rich following chemical enrichment and decreased metal loss. We use a relation between gas-phase metallicity, explicitly the nebular oxygen abundance relative to hydrogen, O/H , and M_{stellar} derived from SDSS galaxies (Tremonti et al. 2004). We use units of $12 + \log(\text{O}/\text{H})$, where the solar abundance is $\simeq 8.69$. This $M_{\text{stellar}} - Z$ rela-

Table 1. Properties for the SNLS, low-redshift and R07 host galaxies. The full table can be found in the electronic version of the journal.

SN Name	z_{cmb}	i_M	LOG M_{stellar} (M_{\odot})	LOG SFR ($M_{\odot}\text{yr}^{-1}$)
03D1ar	0.408	19.57	$10.37^{+0.28}_{-0.10}$	$1.55^{+0.27}_{-0.77}$
03D1au	0.504	21.87	$9.55^{+0.13}_{-0.09}$	$0.63^{+0.58}_{-0.63}$
03D1aw	0.582	22.53	$9.21^{+0.04}_{-0.14}$	$0.87^{+0.03}_{-0.37}$
03D1ax	0.496	18.49	$11.61^{+0.15}_{-0.08}$	< -3.00
03D1bk	0.865	20.21	$11.47^{+0.08}_{-0.03}$	$0.46^{+0.04}_{-3.46}$
03D1bp	0.347	18.72	$10.85^{+0.20}_{-0.05}$	$0.71^{+0.33}_{-0.33}$
03D1co	0.679	23.94	$8.69^{+0.50}_{-0.06}$	$-0.06^{+0.66}_{-0.43}$
03D1dt	0.612	21.91	$9.76^{+0.08}_{-0.11}$	$0.41^{+0.16}_{-0.16}$
03D1ew	0.868	26.37	$8.58^{+0.70}_{-0.91}$	$-0.96^{+1.32}_{-2.04}$
03D1fc	0.332	19.55	$10.41^{+0.02}_{-0.05}$	$0.47^{+0.25}_{-0.24}$

**Figure 1.** The distribution of SN Ia host galaxies in M_{stellar} , SFR and inferred gas-phase metallicity. Left: Histograms in M_{stellar} , SFR, and metallicity; low-redshift (open histogram) versus SNLS (filled histogram). Right: The distribution in the M_{stellar} –SFR plane. The dashed line is a line of constant sSFR used as the default split to separate high sSFR and low sSFR galaxies. The light-grey shaded areas show the range over which the default splitting value is varied in Section 4.2. SNLS SN Ia hosts are shown as filled circles, low-redshift hosts as white circles, R07 hosts as grey circles. Note that the apparent diagonal ridgeline in the M_{stellar} –SFR plane is a result of the maximum sSFR being reached in the model SFHs, a disadvantage of the simple SFHs considered here.

tion is observed to evolve with redshift, being shifted towards high M_{stellar} or lower metallicities at higher redshift (e.g. Savaglio et al. 2005; Lamareille et al. 2009). To account for this effect, we use the evolution measured by Lamareille et al. (2009) relative to the Tremonti et al. (2004) relation. (Note that the use of a M_{stellar} – Z relation that evolves with redshift will exacerbate the difference in M_{stellar} between low redshift and SNLS hosts when expressed as a metallicity.) Though the calibration of nebular-line metallicity diagnostics is a complex topic (e.g. Kewley & Ellison 2008), the *exact* calibration scale does not concern us here, so long as we can place all our hosts on the same relative system to search for variations in the SN sample.

The Tremonti et al. (2004) relation is derived for gas-phase metallicity, and may not be applicable in elliptical galaxies with little cold gas where a stellar metallicity may be more appropriate. In principle, we could also use a stellar metallicity–mass relation (e.g., Gallazzi et al. 2005). However, this relation has only been measured at low-redshift, and any (expected) evolution with redshift has not been

constrained observationally – stellar metallicities are significantly more difficult to measure than gas-phase metallicities, requiring absorption line measures instead of emission lines. Therefore we restrict ourselves to the gas-phase metallicity, but note that as the mechanism for retaining metals is the depth of the galaxy gravitational potential well, ellipticals (or passively evolving galaxies) should follow the same general trend between stellar metallicity and M_{stellar} (Gallazzi et al. 2005), with stellar metallicity and gas-phase nebular metallicity well correlated (e.g. Cid Fernandes et al. 2005; Gallazzi et al. 2005).

The broad-band SED fitting approach used here is a relatively crude way to determine galaxy properties. However, our choice is limited as, for the SNLS sample at least, we only have optical $u_M g_M r_M i_M z_M$ magnitudes (albeit measured from extremely deep and well-calibrated images) and some near-IR information for the hosts. In particular, spectroscopic diagnostics used in many other galaxy analyses are not available. Though each SN Ia does have a spectrum containing some host galaxy spectral information, these form a very heterogeneous set invariably contaminated by SN light,

making the accurate measurement of host spectral features impossible. We did explore adding GALEX ultraviolet data to our SNLS host fits (as in N09); however the relatively poor resolution of the GALEX imaging led to substantial source confusion for most of our galaxies. We also experimented with the use of more complex (“stochastic”) SFHs involving bursts of star formation superimposed on smooth underlying SFHs as in other studies of SN Ia or gamma-ray burst host galaxies (e.g. Savaglio et al. 2009; Schawinski 2009); however the increased number of free parameters (e.g., burst strength, burst duration, burst age, etc.) makes the problem quite degenerate. Hence, our host galaxy parameters are only representative of the dominant star formation episode in each host. We note that the use of stochastic SFHs results in increased derived stellar masses of galaxies by about 0.14 dex (Pozzetti et al. 2007; Lamareille et al. 2009).

Where required in our analysis to examine the dependence of SN Ia properties on environmental properties, we classify the SN Ia host galaxies into different groups. The first split is performed according to their sSFR: galaxies with $\log(\text{sSFR}) < -9.7$ with smaller amounts of star formation relative to their stellar masses are classified as low-sSFR, and those with a larger sSFR are classified as high-sSFR. This split will separate those galaxies dominated by young stellar populations from those comprised of older stellar populations. The second split is based upon the host galaxy M_{stellar} ($\log(M_{\text{stellar}}) > 10.0$ are defined as high mass), with an extension to the inferred gas-phase metallicity ($Z > 8.8$ are defined as metal rich). (We consider the effect of varying these split points in later sections.) Approximately 30 per cent of SNe Ia in our SNLS sample are found in low-sSFR systems according to the definition above.

3 SN IA PROPERTIES AS A FUNCTION OF HOST GALAXY PROPERTIES

In this paper we correct SN Ia peak magnitudes for the stretch and colour relations (m_B^{corr}) using a standard empirical approach with the form:

$$m_B^{\text{corr}} = m_B + \alpha(s - 1) - \beta C \quad (1)$$

where α parametrizes the stretch–luminosity relation, β parametrizes the colour–luminosity relation, and m_B , s and C are the observed peak magnitude, stretch and colour output from the light curve fitters (§ 2.2). m_B and C are corrected for Milky Way extinction but not for any host galaxy extinction. α and β are typically determined from simultaneous fits with the cosmological parameters (e.g. Astier et al. 2006, see also § 4), and reduce the scatter in the peak SN Ia magnitudes to ~ 0.15 mag.

3.1 Light curve shape and colour

The correlation between SN Ia light curve shape (stretch, Δm_{15} , etc.) and host galaxy morphology (e.g. Hamuy et al. 1995, 1996b; Riess et al. 1999; Hamuy et al. 2000), SFR (S06; N09), and M_{stellar} (Howell et al. 2009) is well established: fainter, lower stretch (high Δm_{15}) SNe Ia explode in older stellar populations showing little ongoing star formation.

We extend this earlier work to examine the SN Ia properties as a more continuous function of sSFR and M_{stellar} in Fig. 2. The expected trends with stretch are recovered. Low stretch SNe Ia preferentially explode in low-sSFR galaxies with little or no ongoing star formation, and are rarer in galaxies which have substantial star formation. By contrast the higher stretch SNe Ia are found in galaxies with a range of mean sSFRs but with a deficit in the low sSFR systems. Similar trends are seen as a function of M_{stellar} : lower-stretch SNe Ia are almost entirely absent in low- M_{stellar} galaxies (expected to have the highest sSFRs). There is also evidence for stretch being a continuous variable of sSFR or M_{stellar} .

No conclusive trends between SN Ia rest-frame colour and host galaxy properties have yet been identified. In our data, there are also no strong trends, though SNLS SNe Ia in low sSFR systems do show slightly bluer colours in the mean (no differences are seen between the colours of SNe Ia in low- M_{stellar} hosts and high- M_{stellar} hosts). A t -test shows the mean colours of SNe Ia in low and high sSFR galaxies have about a 97% chance of being different; a Mann-Witney U test gives a similar 97% chance that the colours arise from different distributions. This is consistent with the simple viewpoint that more strongly star-forming galaxies contain more dust, and that dust will make SN colours redder. However, the lack of a large difference in mean colour suggests that the amount of dust along the line of sight to SNe Ia in star-forming host galaxies is small.

Note that the lack of a trend in the opposite sense may also be considered surprising at first sight. There is a strong variation in stretch with star formation activity, and observations show that the very lowest- s (and typically sub-luminous) SNe Ia are usually redder in C – this would imply that the lowest sSFR systems should host the reddest SNe Ia, which is opposite to the weak trend that we do observe. However, the strength of this stretch–colour relationship for “normal” SNe Ia at maximum light is weak (e.g. Jha et al. 2006; Nobili & Goobar 2008; Takahashi et al. 2008). Trends do exist between other colours and stretch and at other light-curve phases (e.g. Phillips et al. 1999; Nobili & Goobar 2008) and for sub-luminous SN1991bg-like very low- s SNe Ia (Garnavich et al. 2004; Jha et al. 2006), but these are excluded from our analysis by the $s > 0.8$ requirement.

4 SN LUMINOSITY DEPENDENCE ON HOST CHARACTERISTICS

We now examine the effect of the environment on the “corrected” brightness of SNe Ia, and hence the effect on their use in a cosmological analysis. We minimize

$$\chi^2 = \sum_N \frac{(m_B^{\text{corr}} - m_B^{\text{mod}}(z, \mathcal{M}_B; \Omega_M))^2}{\sigma_{\text{stat}}^2 + \sigma_{\text{int}}^2} \quad (2)$$

where m_B^{corr} is given by eqn. (1), σ_{stat} is the total identified statistical error and includes uncertainties in both m_B and m_B^{mod} , σ_{int} parametrizes the intrinsic dispersion of each SN, and the sum is over the N SNe Ia entering the fit. m_B^{mod} is the model B -band magnitudes for each SN, given by

$$m_B^{\text{mod}} = 5 \log_{10} \mathcal{D}_L(z; \Omega_M) + \mathcal{M}_B, \quad (3)$$

where \mathcal{D}_L is the c/H_0 reduced luminosity distance with the c/H_0 factor (here c is the speed of light) absorbed into \mathcal{M}_B ,

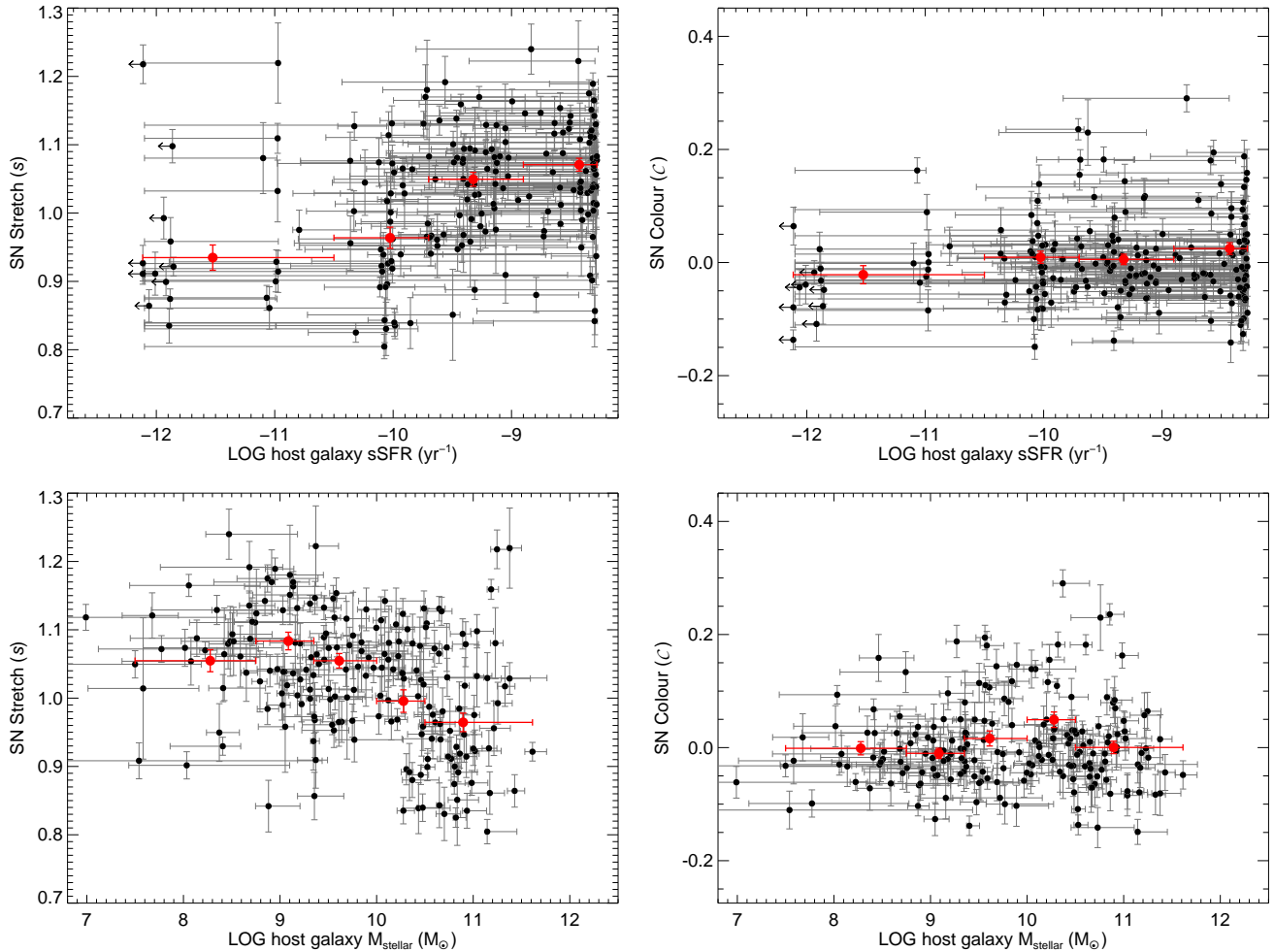


Figure 2. The SN Ia stretch (s ; left panels) and colour (C ; right panels) from SiFTO as a function of the host galaxy sSFR (upper panels) and M_{stellar} (lower panels). The red points show the weighted mean s or C , corrected for dispersion, in bins of sSFR and M_{stellar} . Only SNLS SNe are shown (similar plots for the low-redshift sample can be found in N09). Equivalent results are found with SALT2.

the absolute luminosity of a $s = 1$ $C = 0$ SN Ia (eqn. (1)). Explicitly, $\mathcal{M}_B = M_B + 5 \log_{10}(c/H_0) + 25$, where M_B is the absolute magnitude of a SN Ia in the B -band (for SALT2 fits, M_B refers to an $x_1 = 0$, $C = 0$ event). For convenience, we present our results as M_B rather than \mathcal{M}_B , but note that this requires a value of H_0 to be assumed – a choice that does not impact our results in any way.

α , β and \mathcal{M}_B are often referred to as “nuisance variables” in cosmological fits as they are not of immediate interest when determining cosmological models. Instead they parametrize luminosity variations within the SN Ia samples and are likely related to the physics of the SN Ia explosion and/or the SN Ia environment; clearly this makes them of great interest in this paper.

Two different approaches are used. The first approach examines the residuals of the SNe from global cosmological fits using the SNLS3 $z < 0.85$ plus low-redshift sample, fixing $\Omega_M = 0.256$ (the best-fit value for this sample). We choose this number instead of a more “standard” value like $\Omega_M = 0.3$ to ensure that no redshift bias in our SN Ia residuals is introduced by adopting a cosmological model that does not fit the data adequately. The second examines any

variation of the nuisance variables by fixing the same cosmological model and performing fits on sub-samples of SNLS SNe with the nuisance parameters free. The first technique uses global values of the nuisance variables for the entire sample, whereas the second allows them to vary by environment. The advantage of the latter technique is that as the cosmological model is fixed, a large low redshift sample is not required in order to examine brightness-dependent tests internally within the well-measured SNLS sample. Throughout, we define a Hubble residual as $m_B^{\text{corr}} - m_B^{\text{mod}}$, i.e. brighter SNe have negative Hubble residuals.

4.1 Residuals from global cosmological fits

We consider the residuals from the best fitting cosmological model as a function of three host properties: sSFR, M_{stellar} , and M_{stellar} converted into a metallicity estimate (Z). Residual trends here indicate luminosity-dependent effects that are not removed by the standard s (or x_1) and C methodology, but that do correlate with some other physical variable associated with the host galaxy. We emphasise that M_{stellar} and Z are therefore highly correlated, and our Z estimates

are dependent on the evolution in the $M_{\text{stellar}}-Z$ relation measured by Lamareille et al. (2009).

4.1.1 Host specific SFR

The residuals in the SNLS and low-redshift samples as a function of host galaxy sSFR are shown Fig. 3 (the R07 sample has too few SNe for any meaningful trends to be detected). In the SNLS sample, there is evidence that SN Ia events in low sSFR galaxies appear brighter on average than those in high sSFR galaxies after s/x_1 and \mathcal{C} corrections. The numerical values for the mean residuals in each bin are given in Table 2 for SiFTO and Table 3 for SALT2; the differences seen are not dependent on the light curve fitter used. Note that this trend is opposite to that perhaps expected from the observation that low-stretch (intrinsically fainter) SNe Ia reside in lower-sSFR hosts (§ 3.1); however this observation is pre-stretch correction – our residuals have been corrected for both stretch and colour (this is discussed in more detail in § 5.3).

The differences in the SNLS samples between the two lowest and two highest sSFR bins are $\simeq 2.6\sigma$ significance. In the low-redshift sample analysed here, the trends are consistent with the SNLS sample (discarding the most strongly star-forming bin with only a small number of events), but low significance. For the SNLS data, fitting a straight line to the binned points and accounting for errors in both axes detects a non-zero gradient at $\simeq 2.5\sigma$.

4.1.2 Host stellar mass

The residuals as a function of host galaxy M_{stellar} are shown in Fig. 4. In this case, SNe in more massive galaxies appear brighter on average than those in lower-mass galaxies, after s/x_1 and \mathcal{C} corrections. The mean residuals are given in Tables 2 and 3, middle panel. In the SNLS sample, SNe in the three lowest M_{stellar} bins are fainter than those in the two highest M_{stellar} bins at $\simeq 3.9\sigma$ significance. The low-redshift sample is consistent with this, though again the significance is smaller and the range in M_{stellar} is much more restricted. For the SNLS data, fitting a straight line to the binned points detects a non-zero gradient at $\simeq 3.1\sigma$.

4.1.3 Host inferred metallicity

We convert our M_{stellar} into gas-phase metallicities (Z) as described in § 2.4. The residuals as a function of host galaxy Z are shown in Fig. 5. As the Z estimates are directly related to the M_{stellar} , the same trends are apparent – indeed, had we used an $M_{\text{stellar}}-Z$ relation that did not evolve with redshift (e.g. Tremonti et al. 2004; Gallazzi et al. 2005), the Z and M_{stellar} results would be identical. The mean residuals are given in Table 2 and 3, lower panel. In the SNLS sample, SNe in low- Z galaxies are fainter than those in high- Z galaxies at $\simeq 3.7\sigma$ significance. The low-redshift sample is consistent with this, though the range in Z is more restricted. Fitting a straight line to the binned SNLS points detects a non-zero gradient at $\simeq 3.0\sigma$.

4.2 Universality of the nuisance variables

We now consider the s/x_1 and \mathcal{C} corrections that are applied to the SN magnitudes, and test whether these two corrections are consistent for sub-samples of SNe divided according to the characteristics of their host galaxies. We perform these tests using the larger and more complete SNLS SN Ia sample, and again hold the cosmological model fixed.

As discussed in Section 2.4, we separate the hosts according to their sSFR, M_{stellar} , and Z . The exact values chosen as the split points are a somewhat subjective choice (e.g. Fig. 1). The M_{stellar} split point was chosen to separate the hosts into bins of approximately equal sizes, and the Z split point is this M_{stellar} value converted into a Z at $z = 0.5$; no fine-tuning was attempted. We explore how our results change as we modify the default splits of § 2.4 over a range of 0.8 in $\log(\text{sSFR})$, 1.0 dex in $\log(M_{\text{stellar}})$, and 0.2 dex in Z . We perform fits for α , β and M_B , in each case iteratively adjusting σ_{int} until a χ^2 per degree of freedom of 1.0 is obtained. The SiFTO results are given in Tables 4, 5, and 6.

As expected from § 4.1, there are several host dependent trends. In particular, we find that

- SNe Ia in high- M_{stellar} or high- Z hosts prefer brighter M_B than those in low- M_{stellar} (low- Z) hosts ($\simeq 4.0\sigma$), as do SNe in low-sSFR versus high-sSFR hosts ($\simeq 2.5\sigma$), both in the same sense as the trends in Fig. 3,
- SNe Ia in low-sSFR hosts show smaller values of β than those in high-sSFR hosts ($\simeq 2.7\sigma$). Smaller ($< 2.5\sigma$) differences are also seen between β measured in high and low- M_{stellar} (Z) hosts, though this is more dependent on the split point used,
- The α values in the split samples are consistent, differing only at $< 1.5\sigma$,
- SNe Ia in low-sSFR hosts show a smaller r.m.s. scatter about the best fits than those in high sSFR hosts; the r.m.s. scatter of SNe in high- M_{stellar} (Z) and low- M_{stellar} (Z) hosts are similar,

These results are not sensitive to the split points used to characterise low-sSFR versus high-sSFR, or high- M_{stellar} (Z) versus low- M_{stellar} (Z) hosts. Fig. 6 shows the joint confidence contours in the three combinations of the nuisance variables for the sSFR and M_{stellar} split samples.

We also assess the significance of these results using a Monte-Carlo permutation test of our data. We randomly draw $N_{\text{low-sSFR}}$ (or $N_{\text{high-M}}$ when considering the M_{stellar} split) SNe Ia from the full SNLS sample (without replacement) to generate a fake low-sSFR (high- M_{stellar}) sample with the same number of events as the true low sSFR sample. The $N_{\text{high-sSFR}}$ ($N_{\text{low-M}}$) remaining SNe are assigned to the fake high sSFR (low- M_{stellar}) sample. The nuisance variable fits are repeated on both datasets, and the best-fitting α , β and M_B recorded. We repeat this procedure 25000 times, and compare the distribution of derived nuisance variables from the permuted samples to the values recovered for the real samples. We assess how frequently the difference between the nuisance variables for the fake sample is equal to or greater than the difference between the same parameters measured on the real data. The Monte Carlo approach can also assess the significance of any differences

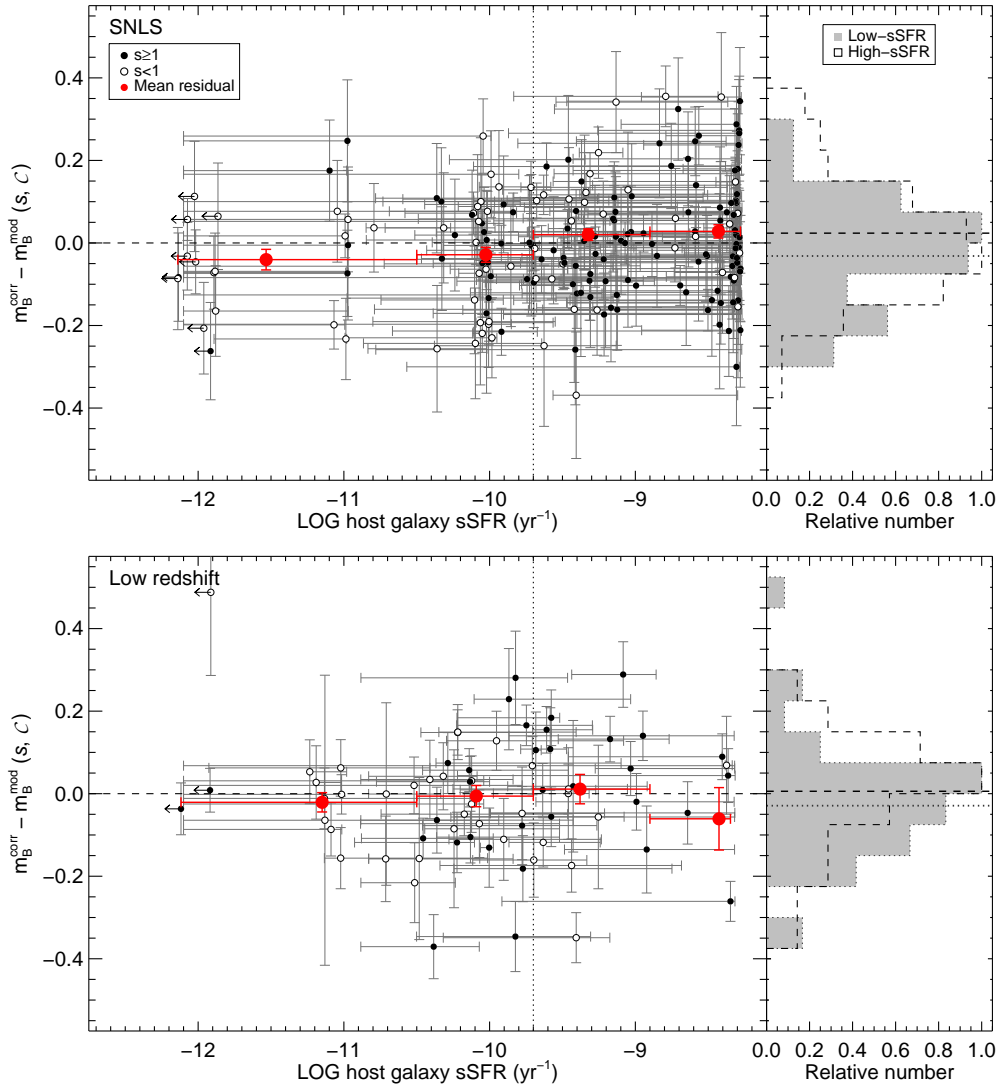


Figure 3. Residuals from the best-fitting cosmology for the SNLS (top) and low redshift (bottom) samples as a function of host galaxy sSFR. Hosts with $s < 1$ SNe Ia are shown as open circles, and those with $s \geq 1$ as filled circles. Brighter SNe Ia after correction have negative residuals. The error bars on the individual SNe are taken from the SED fitting for the sSFR axis, and are the statistical errors propagated through the light curve fitting for the residual axis (i.e. they do not include the σ_{int} component). The red circles are the mean residuals in bins of host sSFR, drawn at the mean value of the sSFR in each bin. The error bars on these points represent the bin width in sSFR, and the weighted error on the mean (corrected for dispersion in each bin) for the residual axis. The right-hand histograms show the total residuals for SNe Ia in low and high sSFR hosts.

seen in r.m.s. scatter between different samples, otherwise difficult to assess statistically.

For samples split by sSFR, we find that the differences in α are found in randomly permuted samples 23% (a $\sim 1.2\sigma$ significance) of the time, for β 2.6% ($\sim 2.2\sigma$), for M_B 0.5% ($\sim 2.8\sigma$) and for the r.m.s. scatter 3.9% ($\sim 2.1\sigma$). For samples split by M_{stellar} , the differences are found in random samples 34% ($\sim 0.95\sigma$) for α , 6.5% ($\sim 1.8\sigma$) for β , 0.005% ($\sim 3.5\sigma$) for M_B , and 44% ($\sim 0.8\sigma$) for the r.m.s.. These results support our main finding above: the most significant differences are seen in M_B for all methods of splitting the host galaxies. Monte Carlo tests show smaller significances in β and r.m.s. scatter for the sSFR split, and the differences in r.m.s. are not significant for samples split by M_{stellar} . For the α parameters no significant differences are seen. Monte

Carlo tests on the Z -split sample are similar to those for M_{stellar} .

4.3 Effect of assumed cosmology

Our choice of cosmology could affect our results in two ways. The first is the impact on the derived absolute host galaxy properties, such as M_{stellar} or sSFR. Changing the assumed H_0 ($70 \text{ km s}^{-1} \text{ Mpc}^{-1}$) has only a superficial effect – all the host galaxy masses or other derived properties will change relative to each other in the same consistent way. Altering the other cosmological parameters, such as Ω_M , has a more subtle effect. In a flat universe, a smaller Ω_M will make the higher-redshift hosts more massive compared to those at lower-redshift (effectively they become more distant); a

Sample	log sSFR (yr^{-1})	All SNe			$s < 1$			$s \geq 1$		
		N	Mean residual	Error	N	Mean residual	Error	N	Mean residual	Error
SNLS	-11.53	22	-0.040	0.025	16	-0.043	0.027	6	-0.025	0.073
	-10.03	43	-0.029	0.018	23	-0.028	0.029	20	-0.029	0.020
	-9.32	59	0.020	0.014	19	0.053	0.027	40	-0.005	0.014
	-8.43	71	0.028	0.016	12	0.084	0.042	59	0.016	0.017
Low- z	-11.15	15	-0.021	0.023						
	-10.09	29	-0.006	0.026						
	-9.38	20	0.011	0.036						
	-8.43	5	-0.061	0.076						

Sample	log M_{stellar} (M_{\odot})	All SNe			$s < 1$			$s \geq 1$		
		N	Mean residual	Error	N	Mean residual	Error	N	Mean residual	Error
SNLS	8.30	27	0.041	0.025	3	0.058	0.074	24	0.037	0.028
	9.09	35	0.021	0.015	7	0.100	0.034	28	-0.001	0.015
	9.61	40	0.048	0.018	11	0.095	0.027	29	0.026	0.023
	10.28	36	-0.023	0.025	13	-0.007	0.050	23	-0.038	0.025
	10.90	56	-0.037	0.014	36	-0.032	0.019	20	-0.049	0.021
Low- z	7.88	2						
	9.01	3	0.115	0.031						
	9.79	6	0.090	0.052						
	10.32	20	0.018	0.030						
	10.94	38	-0.028	0.021						

Sample	Z ($12+\log(\text{O}/\text{H})$)	All SNe			$s < 1$			$s \geq 1$		
		N	Mean residual	Error	N	Mean residual	Error	N	Mean residual	Error
SNLS	8.24	41	0.023	0.018	7	0.042	0.035	34	0.018	0.021
	8.56	35	0.020	0.018	8	0.070	0.060	27	0.011	0.018
	8.72	35	0.059	0.019	8	0.106	0.024	27	0.035	0.024
	8.88	66	-0.034	0.017	35	-0.020	0.026	31	-0.056	0.020
	9.00	15	-0.022	0.022	12	-0.012	0.027	3	-0.051	0.033
Low- z	8.07	2						
	8.55	2						
	8.73	2						
	8.91	5	0.049	0.039						
	9.06	58	-0.015	0.017						

Table 2. Binned SN Ia residuals for the SNLS and low-redshift samples as a function of host galaxy sSFR, M_{stellar} , and Z , calculated with the SiFTO light curve fitter. The host parameter bin centres are given as the mean of all the hosts in that bin. The mean residuals are the weighted average of SNe in each bin, and the errors are the errors on that weighted mean.

larger Ω_M will have the opposite effect. Within the errors to which cosmological parameters are currently measured, this is a small effect – a stellar mass derived with $\Omega_M = 0.30$ instead of $\Omega_M = 0.256$ changes by <0.04 dex at $z = 0.5$ and <0.07 dex at $z = 1$. We have run our fits using this alternative model and find essentially identical results.

The cosmological model could also impact the SN properties. If the redshift distributions of the host galaxies either side of the split point in mass or metallicity are different, then any systematic trend in SN brightnesses with redshift may increase (or decrease) the significance of the differences in the nuisance parameters. For example, an incorrect photometric zeropoint in one of the SNLS filters would introduce a difference in SN Ia brightness which is a smooth function of redshift, and if the mix of hosts also changes with redshift, this could introduce a corresponding offset in the magnitudes of SNe Ia in those hosts.

We test the effect of the assumed cosmology in Fig. 7. We start with our default cosmology ($\Omega_M = 0.256$, $w = -1$), and vary Ω_M (by ± 0.15) and w (by ± 0.4) recording the difference in derived nuisance parameters. As might be expected only small variations in the differences in the de-

rived nuisance parameters are seen. The largest variation in the difference in M_B is with M_{stellar} ($\sim \pm 0.01$), for β with M_{stellar} ($\sim \pm 0.05$), and for α with Z ($\sim \pm 0.05$). Thus the assumption of the cosmological model does not drive our results.

4.4 SNLS selection effects

A final consideration is the possibility of a selection effect which operates to either select against fainter SNe Ia (after correction) in massive or low-sSFR galaxies, or brighter SNe Ia in low- M_{stellar} or high-sSFR galaxies. A mechanism for the latter is difficult to conceive, but for the former possible biases can be imagined. SNe Ia in high- M_{stellar} galaxies will be *intrinsically* fainter (i.e., lower-stretch) and will lie against a brighter host background, decreasing their contrast over their host galaxies. If this operates near the SNLS spectroscopic limit, then we may be biased to preferentially observe the brighter sub-sample of this population in massive galaxies, i.e. those that at fixed light-curve shape are over-luminous (following the σ_{int} distribution).

We have partially mitigated against this selection effect

Sample	log sSFR (yr^{-1})	All SNe				$x_1 < 0$			$x_1 \geq 0$		
		N	Mean residual	Error	N	Mean residual	Error	N	Mean residual	Error	
SNLS	-11.51	21	-0.036	0.029	15	-0.045	0.029	6	0.009	0.093	
	-10.03	37	-0.021	0.022	20	-0.023	0.037	17	-0.020	0.021	
	-9.31	61	0.027	0.014	21	0.042	0.023	40	0.016	0.018	
	-8.39	70	0.027	0.017	14	-0.002	0.040	56	0.034	0.019	
Low- z	-11.36	21	0.017	0.031							
	-10.06	31	-0.007	0.026							
	-9.38	20	0.026	0.035							
	-8.42	6	-0.092	0.076							

Sample	log M_{stellar} (M_{\odot})	All SNe				$x_1 < 0$			$x_1 \geq 0$		
		N	Mean residual	Error	N	Mean residual	Error	N	Mean residual	Error	
SNLS	8.31	25	0.042	0.030	4	0.041	0.069	21	0.042	0.035	
	9.08	32	0.027	0.019	8	0.068	0.035	24	0.012	0.022	
	9.61	39	0.063	0.016	11	0.042	0.029	28	0.073	0.020	
	10.27	32	-0.017	0.024	12	-0.006	0.045	20	-0.026	0.026	
	10.89	60	-0.036	0.018	35	-0.031	0.024	25	-0.045	0.027	
Low- z	7.88	2							
	9.01	3	0.074	0.042							
	9.81	7	0.038	0.063							
	10.30	21	0.021	0.029							
	10.95	45	-0.009	0.023							

Sample	Z ($12+\log(\text{O}/\text{H})$)	All SNe				$x_1 < 0$			$x_1 \geq 0$		
		N	Mean residual	Error	N	Mean residual	Error	N	Mean residual	Error	
SNLS	8.25	38	0.023	0.024	7	0.043	0.042	31	0.016	0.029	
	8.55	30	0.023	0.019	8	-0.047	0.032	22	0.037	0.022	
	8.72	37	0.069	0.017	10	0.064	0.034	27	0.071	0.019	
	8.88	65	-0.023	0.018	32	-0.014	0.028	33	-0.036	0.023	
	9.00	16	-0.037	0.028	12	-0.020	0.035	4	-0.084	0.040	
Low- z	8.07	2							
	8.55	2							
	8.73	2							
	8.92	6	-0.010	0.062							
	9.07	66	-0.000	0.018							

Table 3. As Table 2, but for the SALT2 light curve fitter. Note that the number of SNe Ia in each bin can vary from that in Table 2 due to slightly different SN parameter calls for SiFTO and SALT2.

LOG sSFR split (yr^{-1})	N_{SN}	α	Low sSFR hosts				High sSFR hosts				
			β	M_B	r.m.s.	N_{SN}	α	β	M_B	r.m.s.	
-9.30	96	1.376 \pm 0.128	2.876 \pm 0.159	-19.193 \pm 0.012	0.127	100	1.757 \pm 0.181	3.729 \pm 0.162	-19.126 \pm 0.017	0.143	
-9.50	74	1.305 \pm 0.148	2.928 \pm 0.184	-19.196 \pm 0.015	0.123	122	1.771 \pm 0.161	3.567 \pm 0.148	-19.130 \pm 0.015	0.151	
-9.70	61	1.379 \pm 0.148	2.728 \pm 0.231	-19.208 \pm 0.016	0.120	135	1.576 \pm 0.149	3.445 \pm 0.136	-19.149 \pm 0.014	0.147	
-9.90	53	1.338 \pm 0.170	2.719 \pm 0.232	-19.204 \pm 0.018	0.123	143	1.576 \pm 0.145	3.455 \pm 0.136	-19.152 \pm 0.013	0.145	
-10.10	27	1.582 \pm 0.255	2.976 \pm 0.451	-19.205 \pm 0.026	0.128	169	1.394 \pm 0.114	3.372 \pm 0.125	-19.167 \pm 0.011	0.142	

Table 4. SiFTO fits with a fixed cosmological model for low and high sSFR galaxies with different values of sSFR (given in column one) used to split the sample. The nuisance parameters are free in the fit.

LOG M_{stellar} split (M_{\odot})	N_{SN}	α	High- M_{stellar} hosts				Low- M_{stellar} hosts				
			β	M_B	r.m.s.	N_{SN}	α	β	M_B	r.m.s.	
9.50	120	1.443 \pm 0.138	3.380 \pm 0.143	-19.189 \pm 0.013	0.142	75	1.660 \pm 0.189	3.601 \pm 0.250	-19.117 \pm 0.020	0.147	
9.75	103	1.501 \pm 0.143	3.258 \pm 0.154	-19.199 \pm 0.014	0.141	92	1.612 \pm 0.173	3.644 \pm 0.188	-19.122 \pm 0.017	0.146	
10.00	92	1.554 \pm 0.148	3.159 \pm 0.163	-19.206 \pm 0.014	0.141	103	1.638 \pm 0.164	3.714 \pm 0.170	-19.121 \pm 0.016	0.143	
10.25	77	1.555 \pm 0.162	3.203 \pm 0.180	-19.213 \pm 0.016	0.143	118	1.673 \pm 0.159	3.499 \pm 0.156	-19.127 \pm 0.015	0.141	
10.50	56	1.577 \pm 0.165	2.937 \pm 0.195	-19.222 \pm 0.017	0.131	139	1.515 \pm 0.141	3.480 \pm 0.145	-19.148 \pm 0.013	0.142	

Table 5. As Table 4, but for M_{stellar} instead of sSFR.

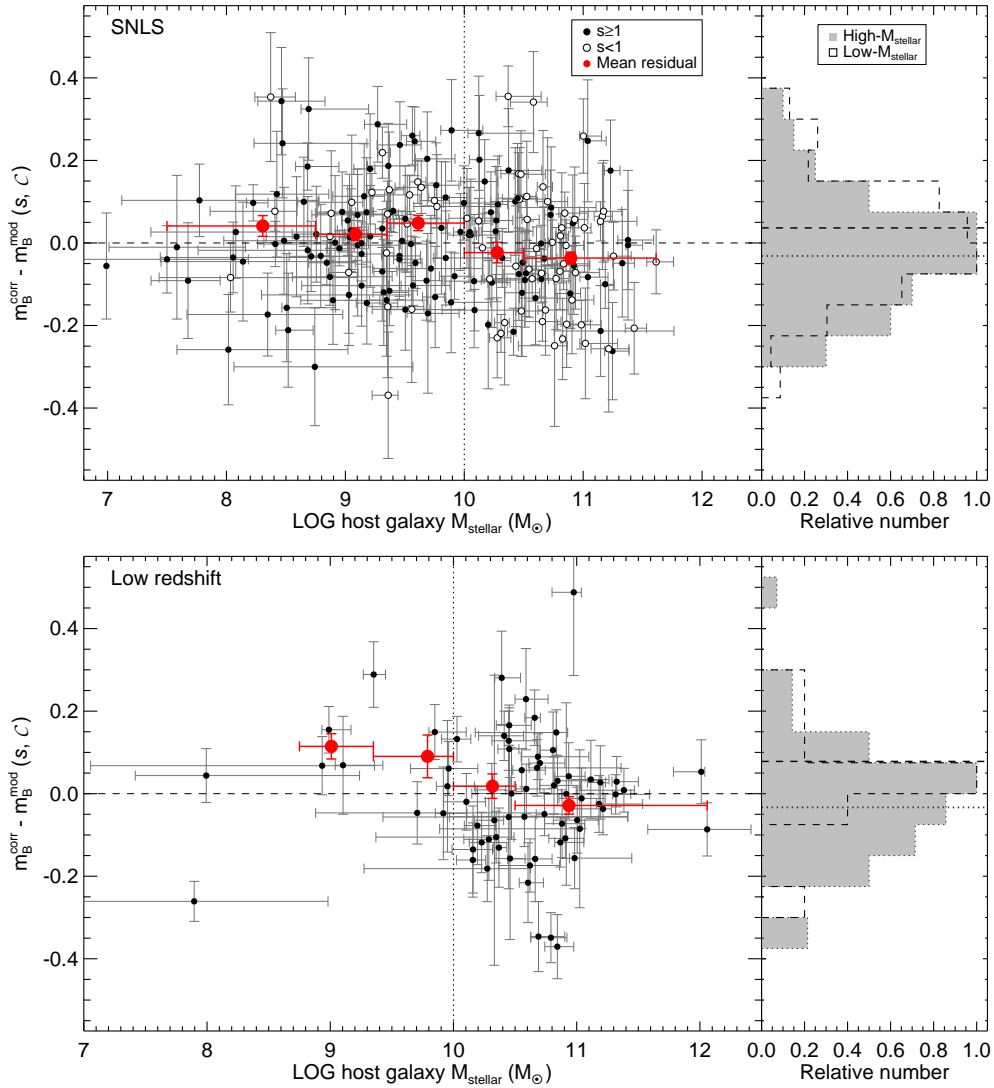


Figure 4. As Fig.3, but for M_{stellar} instead of sSFR.

Z split ($12+\log(\text{O}/\text{H})$)	N_{SN}	α	High- Z hosts			Low- Z hosts				
			β	M_B	r.m.s.	N_{SN}	α	β	M_B	r.m.s.
8.70	102	1.512 ± 0.147	3.238 ± 0.158	-19.195 ± 0.014	0.142	93	1.661 ± 0.175	3.800 ± 0.192	-19.115 ± 0.018	0.149
8.75	92	1.577 ± 0.152	3.172 ± 0.165	-19.204 ± 0.015	0.143	103	1.688 ± 0.161	3.848 ± 0.176	-19.110 ± 0.016	0.146
8.80	81	1.601 ± 0.155	3.102 ± 0.170	-19.210 ± 0.015	0.139	114	1.612 ± 0.160	3.747 ± 0.165	-19.124 ± 0.015	0.144
8.85	61	1.534 ± 0.185	3.095 ± 0.194	-19.217 ± 0.018	0.139	134	1.739 ± 0.148	3.614 ± 0.151	-19.125 ± 0.014	0.143
8.90	34	1.526 ± 0.187	2.795 ± 0.225	-19.218 ± 0.021	0.113	161	1.491 ± 0.130	3.619 ± 0.139	-19.151 ± 0.012	0.148

Table 6. As Table 4, but for Z instead of sSFR.

by restricting our analysis to those SNe Ia lying at $z < 0.85$, away from the redshift limit of SNLS. The total Malmquist bias (including spectroscopic selection) on our SNe below this redshift is < 0.015 mag (Perrett et al. 2010), compared with the size of the magnitude difference in our results of ~ 0.1 mag. We have also tested for the existence of this observational selection effect by examining the SN Ia residuals versus the percentage increase of the SN flux over its host. Below a percentage increase of 100% (i.e., the SN is as bright

as the host measured through a small aperture), identification becomes more difficult (e.g. Howell et al. 2005). Our key diagnostic would be to see brighter SNe (after correction) when the percentage increase is $< 100\%$, and fainter SNe at percentage increases $> 100\%$, if this selection effect were serious. We show these data in Figure 8. No effect is present in our data; only weak trends are present with the percentage increase as expected given the weak correlation with M_{stellar} .

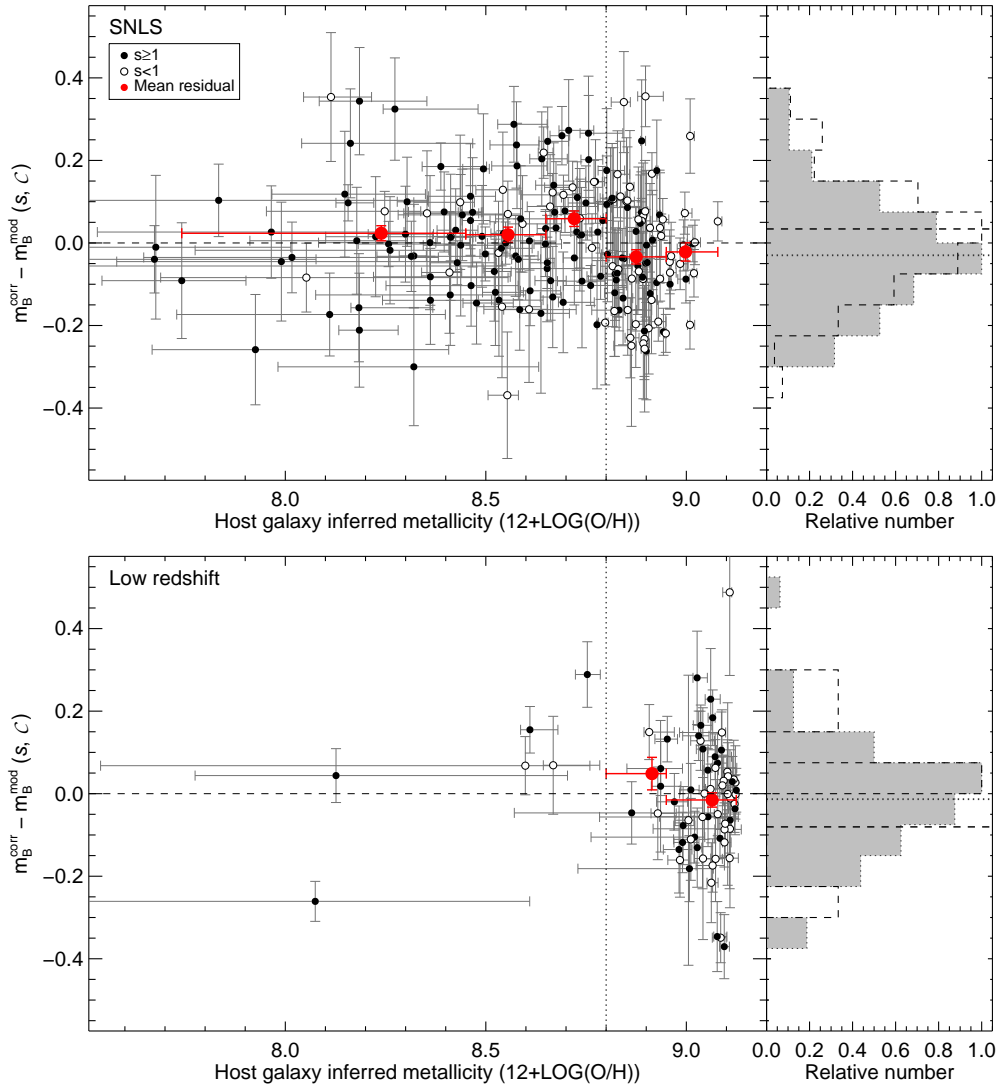


Figure 5. As Fig.3, but for metallicity instead of sSFR.

As a final test, we have also examined the Hubble residuals of events which were not followed spectroscopically by SNLS, but which were subsequently located in an offline search of the same data (Bazin et al. 2009) and are photometrically similar to SNe Ia (Bazin et al., in prep.). The number of additional small percentage-increase objects at $z < 0.85$ is only 24 ($\sim 10\%$ of our total sample), and have the same host-dependent trends as those presented in this paper. We therefore conclude that this potential selection effect cannot drive our results.

5 DISCUSSION

5.1 Comparison to other results

The results of § 4 can be compared to several studies from the literature. The result that high- M_{stellar} galaxies host the brightest SNe Ia after correction was also found by Kelly et al. (2009) at a $\simeq 2.5\sigma$ significance using a similar low-redshift SN Ia sample to that used here.

Using galaxy morphologies for the same low-redshift sample, Hicken et al. (2009b) found weak trends with host galaxy type: SNe Ia in Scd/Sd/Irr galaxies are fainter than those in elliptical galaxies after correction (2σ difference), and have a smaller r.m.s. scatter and lower reddening. Assuming that sSFR closely tracks galaxy morphology, we find a similar effect in that fainter SNe are located in high sSFR galaxies, but we do not reproduce their result that SNe in spiral galaxies have a smaller scatter on the Hubble diagram; in fact our SNLS data suggest the opposite, and at low-redshift we see no significant difference in r.m.s. scatter. We also see no evidence that SNe in spirals have less reddening; SNe in spirals appear redder than those in ellipticals.

Turning to metallicities, Gallagher et al. (2005) used spiral galaxy emission line measurements to directly measure $\log(\text{O}/\text{H})$ for 16 local host galaxies containing SNe for which a Hubble residual was available, but found no significant trend – their results indicated that brighter SNe after correction may lie in more metal rich galaxies, but only at 90% confidence. Gallagher et al. (2008) used another small sample (17 host galaxies) of local SNe in E/S0 galaxies, us-

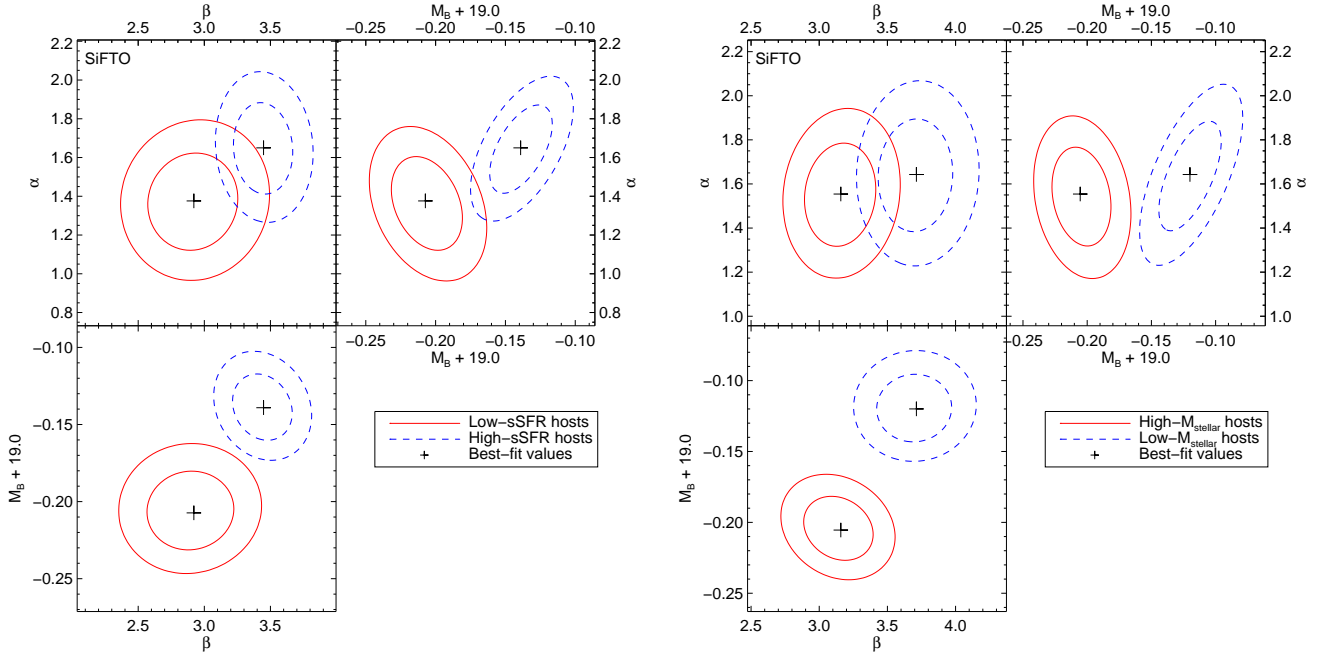


Figure 6. Joint confidence contours (one and two σ) in α and β (top left), α and M_B (top right), and M_B and β (lower left) for fits where the SNe are split according to host galaxy sSFR (left panels) and M_{stellar} (right panels). Plots with SNe split by Z are similar to those for M_{stellar} and are not shown. The crosses show the best fit values.

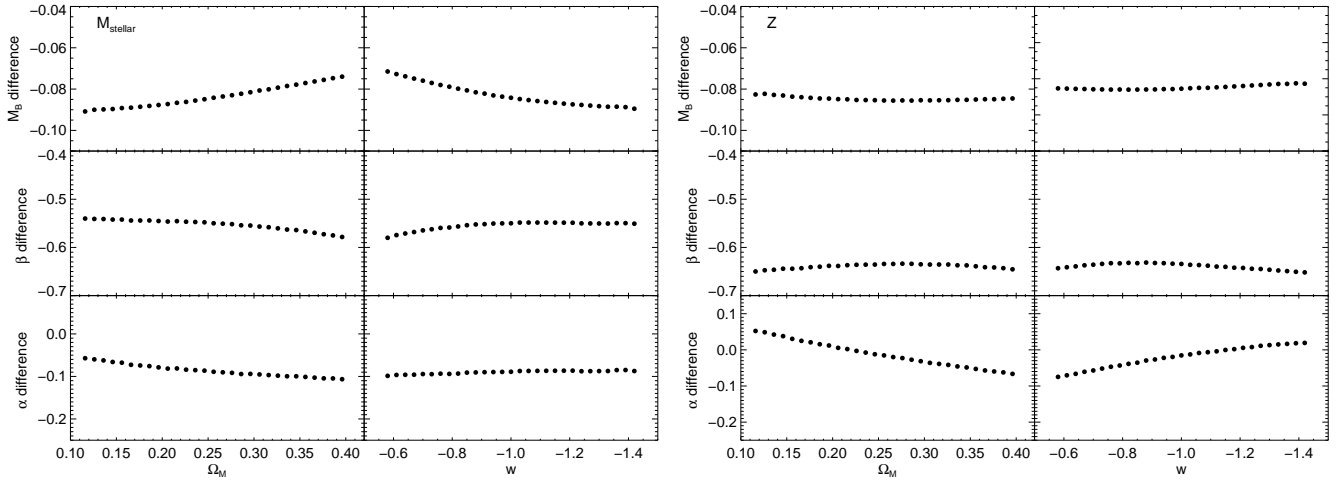


Figure 7. The effect of the assumed cosmology on the differences in nuisance parameters derived from SNe Ia located in hosts either side of the default split points. The left-hand figure shows SN Ia hosts split by M_{stellar} , the right-hand figure by Z . Either Ω_M or w is altered, with the other parameters held fixed, and the difference in nuisance parameters derived from SNe Ia in low- M_{stellar} and high- M_{stellar} (or low- Z and high- Z) hosts plotted.

ing $[M/H]$ spectral measures to show that brighter SNe Ia (again, after correction) were hosted by more metal rich systems with $\simeq 98\%$ confidence.

Howell et al. (2009) previously used 55 SNLS SNe Ia and techniques similar to those in this paper, but found a correlation between Hubble residual and inferred host metallicity (or M_{stellar}) at only $\simeq 1.3\sigma$. These 55 events are also included in this paper, but note that the Hubble residuals of Howell et al. (2009) were based on photometry, calibration and light-curve fitting tools used in Astier et al. (2006) – these have all since improved (see discussions in Guy et al.

2007; Conley et al. 2008; Regnault et al. 2009; Guy et al. 2010). The slope of Hubble residual with inferred $\log(O/H)$ as measured by Howell et al. (2009) is -0.10 ± 0.07 ; fitting the binned points in the SNLS–metallicity plot in Fig. 3 gives a slope of -0.18 ± 0.06 , consistent with Howell et al. (2009) at $\sim 1.5\sigma$.

In summary, some similar trends to those presented in this paper have been found in the past, but all at quite low significance. This is the first dataset where a dependence of corrected SN Ia luminosities on host properties has been definitively detected at $>3\sigma$ confidence.

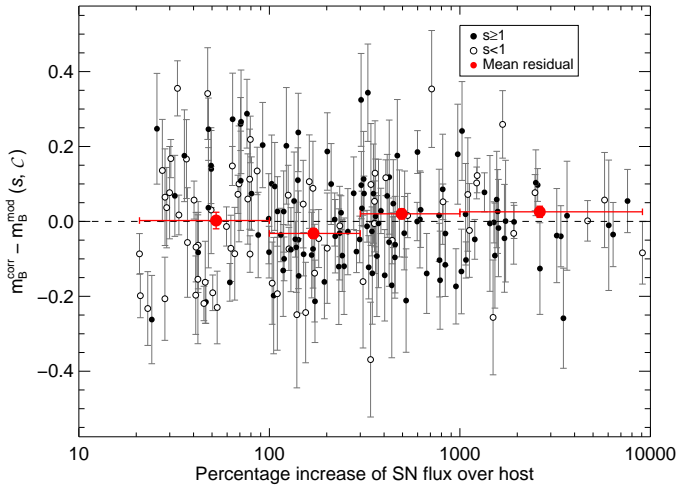


Figure 8. Residuals from the best-fitting cosmology for the SNLS SNe Ia as a function of the percentage increase of the events over their host galaxies at the time of spectroscopic observation. SNe Ia with $s < 1$ are shown as open circles, and those with $s \geq 1$ as filled circles. Brighter SNe Ia after correction have negative residuals. The red circles are the mean residuals in bins of percentage increase, drawn at the mean value of the percentage increase in each bin. The error bars on these points represent the bin width in percentage increase, and the weighted error on the mean for the residual axis.

5.2 Colour residuals

The Hubble residuals as a function of colour for SNLS SNe Ia segregated by the sSFR and M_{stellar} of their hosts are shown in Fig. 9, with the best-fitting relations over-plotted. The (few) objects with red colours could influence the best-fitting β disproportionately. We repeat the nuisance variable fits, each time reducing the maximum allowed colour by 0.05 and re-examining the fit β (Table 7). Clearly the errors in β increase as the redder SNe are excluded due to the reduced baseline in colour.

The difference between the β in low and high sSFR galaxies becomes less significant as the reddest allowed SN Ia colour is reduced – most of the difference seems caused by the reddest SNe Ia. Though the colour variation in SNe Ia is not well understood, high sSFR galaxies are likely to show a larger range in dust content than low sSFR galaxies, and hence display a larger scatter and/or steeper colour–luminosity relations for redder SNe Ia. Removing these redder events is likely to minimise the effect of any difference in β between host galaxy types. It may also be the case that the colour–luminosity relation of the reddest SNe is dominated by the effects of dust rather than intrinsic variation (in which case $\beta \sim R_B$), and hence redder SNe favour larger values of β . We note that Folatelli et al. (2010) actually find an decrease in R_V ($R_V = R_B - 1$) in a sample of low-redshift SNe Ia when including very red SNe Ia, though these events with $(B - V) \sim 1$ are much redder than any SNLS SN considered in this paper. They speculate that this difference in R_V in the reddest SNe Ia could be a result of circumstellar dust (see also Wang 2005).

With smaller maximum allowed colours, the r.m.s. scatter of the fits of SNe Ia in each type are also more consistent. Under the hypothesis that the reddest SNe Ia are the most

affected by dust this might be expected. SN Ia host galaxies are likely to display a range in effective R_V – the Galactic average is 2.99 ± 0.27 (e.g. Fitzpatrick & Massa 2007), and there is no reason to expect the range present in SN Ia hosts to be smaller. For an $E(B - V)$ of 0.1, this would generate an additional scatter of 0.06 mag in SN peak luminosities compared to a SN Ia with a colour excess of zero.

5.3 SN stretch or host dependence?

Given the dependence of SN Ia stretch on host galaxy parameters such as M_{stellar} and sSFR (Fig. 2), the trends of SN Ia brightness with the same parameters (Fig. 3) could simply arise from an incomplete stretch–luminosity correction, rather than an intrinsic dependence on any third variable beyond stretch and colour. For example, if the stretch–luminosity relation were more complex than a simple linear trend but only a linear variable were fit, this could manifest as a dependence of corrected SN Ia luminosity on host galaxy parameters.

We investigate this in two ways. We first examine the luminosity trends as a function of host galaxy parameters segregated by stretch. The SNe Ia plotted in Fig. 2 are coded according to the stretch of the event, and the residuals of both $s < 1$ and $s \geq 1$ SNLS SNe Ia are given in Table 2 (Table 3 has the SALT2 equivalent). Generally, the same trends with M_{stellar} , Z and sSFR are seen for high- s and low- s SNe Ia, though clearly the significance is smaller than for the entire population given the number of events is reduced.

We also experiment with a quadratic stretch–luminosity term in an attempt to remove the host dependence. We add an additional term to eqn. (1) of the form $\alpha_2(s - 1)^2$, shown in Fig. 10. The improvement in the quality of the fits with this extra stretch term is not significant (Table 8) and does not remove the host-dependent SN Ia luminosity trends. These tests suggest that the trends of SN Ia luminosity with host parameters are largely independent of SN Ia stretch.

5.4 Cosmological implications

Differences in mean SN Ia properties when split by host galaxy properties, which are not removed by corrections currently employed in cosmological analyses, could clearly lead to systematic errors in cosmological analyses. Observationally, SNe Ia in massive galaxies appear brighter than those in less massive galaxies – a similar effect is seen when considering sSFR, with SNe Ia in low sSFR galaxies brighter than those in high sSFR galaxies. These differences are significant at $>3\sigma$.

Evidence for two populations of SNe Ia with different photometric properties is not by itself alarming, as the nuisance variables in any global fit will average to values appropriate for the combination of SNe Ia. However, any change in the mix of SNe Ia with redshift could introduce a serious effect. We measure the change in SN Ia host M_{stellar} or Z as a function of redshift (Fig. 11) using the SNLS dataset unrestricted in redshift range, and the low redshift and R07 data. We measure the fraction of host galaxies with M_{stellar} or Z less than the split points defined in earlier sections in each redshift bin. We then make a simple linear fit to these values as a function of redshift i.e., $a + bz$, where a and b are

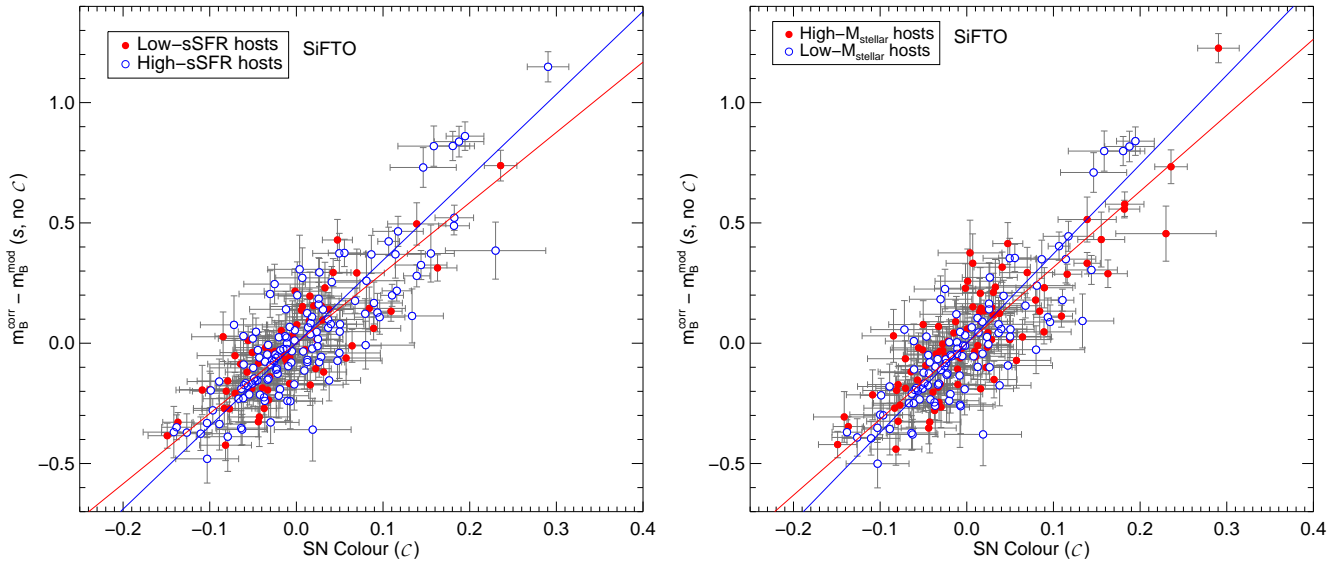


Figure 9. Hubble diagram residuals as a function of C for SNLS SNe Ia before the colour–luminosity relation is applied, split by sSFR (left) and M_{stellar} (right), with the cosmological model fixed and the nuisance variables α , β , and M_B allowed to vary according to the type of host. The over-plotted lines show the best fitting relations (a slope of β). Note that the exact values of the residuals vary between the sSFR and M_{stellar} splits as the nuisance variables are allowed to change. As each set of hosts is allowed to have different values of M_B , the differences in SN Ia luminosity between different host types is not present.

Reddest C permitted	N_{SN}	α	Low sSFR hosts		r.m.s.	N_{SN}	α	High sSFR hosts		r.m.s.
			β	M_B				β	M_B	
0.30	65	1.377 ± 0.158	2.730 ± 0.228	-19.208 ± 0.016	0.120	131	1.573 ± 0.150	3.444 ± 0.137	-19.149 ± 0.014	0.147
0.25	65	1.377 ± 0.158	2.730 ± 0.228	-19.208 ± 0.016	0.120	130	1.521 ± 0.150	3.361 ± 0.142	-19.152 ± 0.014	0.145
0.20	64	1.373 ± 0.158	2.730 ± 0.228	-19.208 ± 0.016	0.120	129	1.549 ± 0.151	3.443 ± 0.152	-19.149 ± 0.014	0.143
0.15	63	1.435 ± 0.164	2.947 ± 0.264	-19.202 ± 0.016	0.123	122	1.614 ± 0.145	3.214 ± 0.183	-19.149 ± 0.013	0.137
0.10	61	1.548 ± 0.170	3.346 ± 0.328	-19.190 ± 0.017	0.129	113	1.600 ± 0.148	3.617 ± 0.257	-19.136 ± 0.014	0.140

Table 7. As Table 4, but testing the effect of the reddest SNe Ia on the derived nuisance variables. Similar results are found for SALT2 fits.

the fit coefficients. To guard against selection effects, we perform the fits with and without the low-redshift data where the selection effects are quite different to those in the SNLS data. In the case of metallicity, the strength of any redshift trend is driven by the form of the M_{stellar} –metallicity relationship assumed – our default relation that evolves with redshift leads to a correspondingly larger redshift trend than a relation that is assumed constant with redshift (and also leads to a decreasing upper metallicity limit for any given redshift, as seen in Fig. 11). If a relation with no redshift evolution is used, the metallicity–redshift plot becomes essentially the same as the M_{stellar} –redshift plot.

As expected from a consideration of popular galaxy formation models, the host galaxies at higher redshift contain, on average, less stellar mass and consequently are likely to be of lower metallicity. The strength of the evolution is most significant with metallicity in the SNLS+R07 data, but is substantially strengthened in M_{stellar} if the low-redshift host data are also included. However, including the low-redshift data is likely to overestimate the strength of the real physical evolution, as the bulk of the low-redshift is strongly biased against host galaxies of low stellar mass. It would be appropriate to include the low-redshift data if the amount of

evolution likely in current cosmological samples was required to be estimated.

Given the expectation and evidence of evolution, either from selection effects or an underlying physical effect, we investigate methods for accounting for it in cosmological analyses, and the effect that it would have if left uncorrected.

5.4.1 Additional nuisance variables

We consider two ways to include additional parameters in the fits. The first and most obvious is to include a further linear $\gamma \times x$ term to eqn. (1), where x is a variable such as M_{stellar} , Z or sSFR measured from the SN Ia host galaxies. The second is motivated by the idea of two populations of SNe Ia rather than a continuum in properties, and instead introduces two independent values for M_B in eqn. (3) for SNe Ia located in different types of host galaxy. Explicitly, SNe Ia located in galaxies with $\log(M_{\text{stellar}}) \geq 10.0$ (or $Z \geq 8.8$, or $\log(\text{sSFR}) \leq -9.7$) are assigned M_B^1 , and SNe Ia in galaxies with $\log(M_{\text{stellar}}) < 10.0$ (or $Z < 8.8$, or $\log(\text{sSFR}) > -9.7$) are assigned M_B^2 . In principle, different values of α and β could also be fit for SNe Ia lying either side of the split point. However, the results of § 4.2

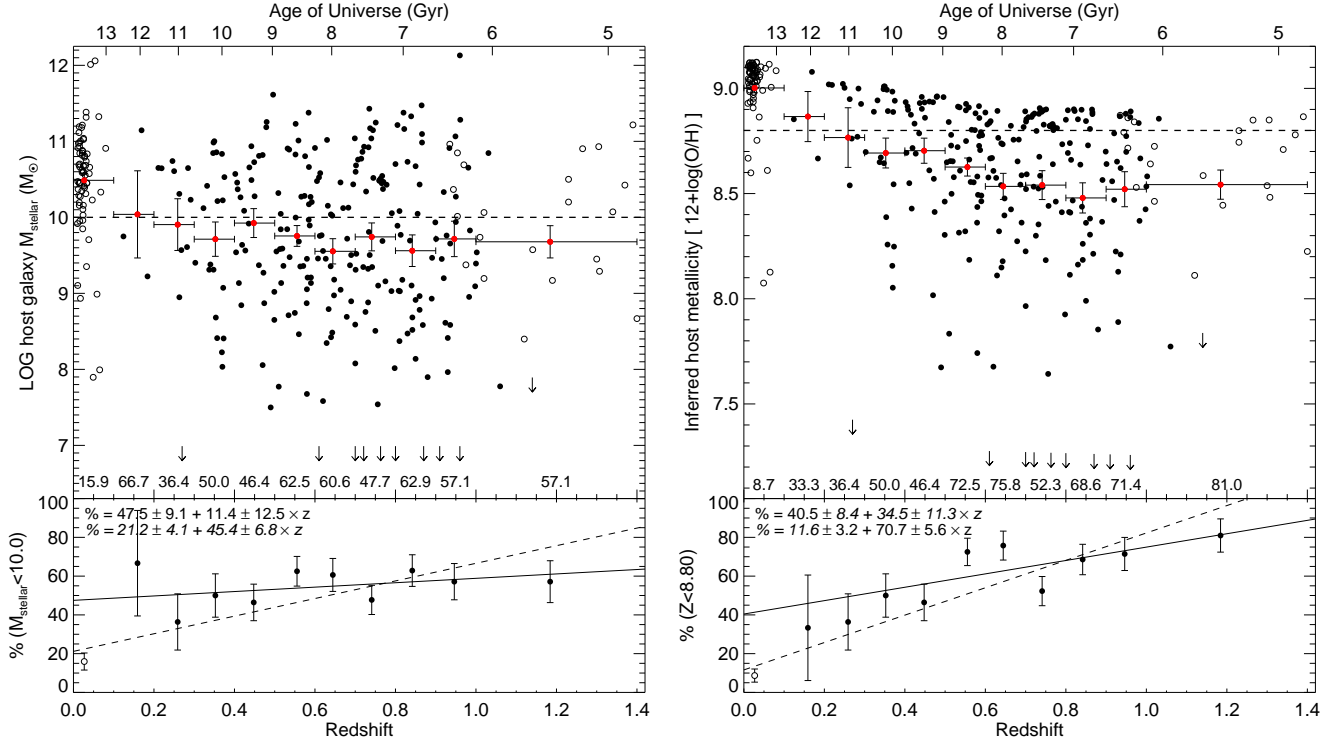


Figure 11. The change with redshift in SN Ia host galaxy M_{stellar} (left) and inferred Z (right). The mean values in bins of redshift are shown as red circles, drawn at the mean redshift in each bin, and with error bars representing the bin width for the redshift axis, and the error on the mean in the M_{stellar} and Z axis. The horizontal dashed lines show the split points used in § 4. Open circles refer to the low redshift or R07 samples, and filled circles the SNLS sample. Note that the differences between the low-redshift and SNLS hosts is unlikely to be a real physical effect, and is generated by selection effects in the low-redshift sample. The lower panels show simple linear fits to the fraction of SN Ia hosts with $\log(M_{\text{stellar}}) < 10.0$ (or $Z < 8.8$), including (dashed line) and excluding (solid line) the low-redshift data (shown as an open circle). The fit parameters are shown; the numbers in italics include the low-redshift data.

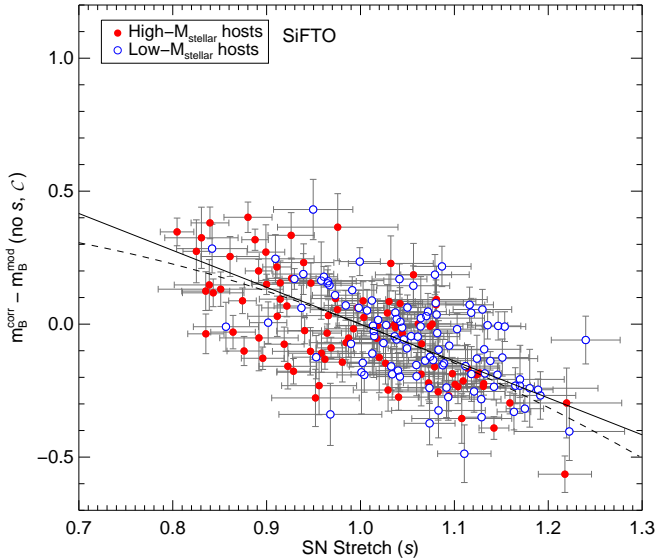


Figure 10. Hubble diagram residuals as a function of s for SNe Ia split by M_{stellar} before the stretch-luminosity relation is applied. The over-plotted lines show the best fitting linear (solid) and quadratic (dashed) stretch-luminosity relations (Table 8). Only a single M_B is used, and so the SNe in high- M_{stellar} and low- M_{stellar} hosts are slightly offset.

show that these nuisance variables are more consistent than M_B , i.e. the M_B captures most of the host galaxy dependent variation.

The results of these different fits with the three different host variables are given in Table 8 (again, the cosmology is held fixed). We also hold σ_{int} fixed, so the addition of an extra parameter into these fits leads to a significant reduction in χ^2 , particularly for the M_{stellar} and related metallicity fits. F -tests show that the addition of an extra parameter improves the quality of the fits beyond that expected by the addition of the extra parameter. For the two M_B fits, the significance is 3.9 – 4.4σ for M_{stellar} and 4.1 – 4.4σ for Z . The linear fit, though still improving the χ^2 , generally performs more poorly: 3.3 – 3.5σ for M_{stellar} and 2.6 – 3.0σ for Z . Fits for two M_B using M_{stellar} or Z perform better than those with sSFR; note that the linear fits in sSFR are difficult to implement as a zero SFR cannot be represented in $\log(\text{sSFR})$ and must be assigned a fixed nominal value.

In the SNLS plus low-redshift fits with two M_B , M_B^2 is more poorly measured than M_B^1 . This can be traced to the biased nature of the low-redshift sample. In SN Ia only fits, the absolute magnitudes are heavily influenced by the low-redshift data where the SN Ia brightness is less dependent on the cosmology, and as there are far fewer SNe Ia in the low-redshift sample in the low- M_{stellar} /low- Z group, the statistical precision of M_B^2 is correspondingly reduced compared to M_B^1 where there are abundant low-redshift SNe Ia.

Sample	α	β	γ or α_2	M_B or M_B^1	M_B^2	χ^2	DOF
Base fits:							
SNLS	1.384±0.103	3.348±0.124	...	-19.170± 0.010	...	190.8	192
SNLS+low- z	1.353±0.083	3.127±0.100	...	-19.178± 0.008	...	270.4	261
SNLS, two α	1.349±0.107	3.347±0.124	1.094±0.943	-19.160± 0.011	...	189.8	191
SNLS+low- z , two α	1.346±0.083	3.121±0.101	0.572±0.733	-19.172± 0.008	...	270.0	260
M_{stellar} fits:							
SNLS, γ	1.553±0.115	3.365±0.127	0.0423± 0.0125	-19.172± 0.010	...	179.9	191
SNLS, two M_B	1.571±0.115	3.382±0.127	...	-19.209± 0.015	-19.127± 0.015	176.0	191
SNLS+low- z , γ	1.515±0.093	3.150±0.103	0.0412± 0.0106	-19.176± 0.009	...	256.4	260
SNLS+low- z , two M_B	1.508±0.091	3.178±0.103	...	-19.211± 0.011	-19.132± 0.014	251.4	260
Metallicity fits:							
SNLS, γ	1.521±0.116	3.398±0.129	0.1124± 0.0412	-19.180± 0.011	...	184.3	191
SNLS, two M_B	1.587±0.116	3.377±0.127	...	-19.214± 0.015	-19.127± 0.015	175.2	191
SNLS+low- z , γ	1.482±0.092	3.184±0.104	0.1107± 0.0328	-19.181± 0.009	...	261.0	260
SNLS+low- z , two M_B	1.520±0.092	3.172±0.103	...	-19.212± 0.011	-19.132± 0.014	250.9	260
sSFR fits:							
SNLS, γ	1.580±0.115	3.254±0.127	-0.0438± 0.0118	-19.176± 0.010	...	178.4	191
SNLS, two M_B	1.525±0.113	3.295±0.125	...	-19.210± 0.017	-19.144± 0.013	182.2	191
SNLS+low- z , γ	1.541±0.094	3.078±0.102	-0.0434± 0.0101	-19.181± 0.009	...	253.7	260
SNLS+low- z , two M_B	1.470±0.090	3.107±0.101	...	-19.211± 0.013	-19.152± 0.012	259.6	260

Table 8. Fits involving extra nuisance parameters based on host galaxy measurements, specifically M_{stellar} , Z and sSFR. In all cases the cosmology is held fixed.

The use of two absolute magnitudes has other advantages over a linear host parameter term. There is no theoretical reason to suppose that any dependence on metallicity be linear; Timmes et al. (2003) show that the putative effect will be strongly non-linear. From a practical viewpoint, the use of two absolute magnitudes is substantially less sensitive to systematics in host galaxy parameter determination. The categorisation of low- M_{stellar} versus high- M_{stellar} is not sensitive to systematic errors associated with the choice of base SED library or assumptions about IMF or dust extinction, nor to the statistical errors on the masses, particularly at low- M_{stellar} where these can be considerable.

The other nuisance parameters are quite stable to the introduction of a γ or M_B^2 term. β is almost unchanged, and α tends to drift to larger values by about 0.15. This latter effect can be understood when considering the stretch dependence on host galaxy properties. Though the trends in SN Ia brightness are the same for both low and high stretch SNe (§ 5.3), lower- s SNe Ia are more prevalent in massive and low sSFR galaxies. These SNe Ia prefer a brighter M_B than those in low- M_{stellar} hosts, making their Hubble residuals, when fitting for two M_B , more positive (fainter). This in turn will lead to a systematic steepening of the stretch–luminosity relation, which is reflected in the larger values of α seen when using third parameters.

5.4.2 Systematics in cosmology

What is the size of the effect of this host galaxy dependence in cosmological analyses? We analyse this by fitting the low-redshift, SNLS and R07 data (314 SNe Ia) with two simple cosmological models with and without the host galaxy term, and assessing the variation of the fit parameters. For simplicity, we use only the statistical errors of the SNe – in a full cosmological analyses, the covariance matrix between differ-

ent SNe accounting for all systematic errors should be used (Conley et al. 2010); here we only aim to assess the size of the effect. Our cosmological models are a flat, Λ CDM model (fitting only for Ω_M , i.e. assuming a constant $w = -1$), and one in which w is still constant but not required to be equal to -1 (fitting for Ω_M and w). In each case the σ_{int} for each SN sample is adjusted to give a reduced χ^2 of 1.0. We also show the effect of adding external constraints into the fit using the Baryon Acoustic Oscillation (BAO) constraints of Eisenstein et al. (2005). The fit results, expressed as a shift in the cosmological parameters from their values without the host parameter, can be found in Table 9. We use the `cosfitter` program², written by one of us (AC) and adjusted to fit for two M_B , to perform the fits. We test both M_{stellar} and gas-phase Z as the third variable on which to split the data.

The size of the effect – the shift in the cosmological parameters with a third variable – is comparable to the simple statistical precision (Table 9). These shifts are larger when metallicity is the third variable ($> 1\sigma$) instead of M_{stellar} ($< 1\sigma$). One source of systematic error is the choice of split point in the host variable. We investigate the dependence of the cosmological results on this choice in Fig. 12. We show the effect on w (including BAO constraints) and the χ^2 as the split point is varied. The median error in mass is $\simeq 0.14$ dex ($\simeq 0.03$ once converted to gas phase Z), and the relative change in w as the split points are varied over this range is small. One approach would be to iterate on the split point in cosmological fits in order to find the model with the smallest χ^2 .

As a final point, we note that the difference in β between low-sSFR and high-sSFR host galaxies, and a change

² http://qold.astro.utoronto.ca/conley/simple_cosfitter/

Third variable	Λ CDM		w model, SN only				w model with BAO			
	$\delta\Omega_M$ (σ)	$\delta\Omega_M$ (σ)	δw (σ)	M_B^1	M_B^2	$\delta\Omega_M$ (σ)	δw (σ)	M_B^1	M_B^2	
M_{stellar}	0.012 (0.6)	0.068 (0.8)	0.173 (0.8)	-19.12 \pm 0.03	-19.19 \pm 0.02	0.001 (0.1)	0.040 (0.6)	-19.13 \pm 0.02	-19.20 \pm 0.02	
Z	0.031 (1.6)	0.066 (0.8)	0.205 (1.0)	-19.10 \pm 0.03	-19.19 \pm 0.02	0.006 (0.3)	0.078 (1.2)	-19.11 \pm 0.02	-19.20 \pm 0.02	

Table 9. Simple effect of a host galaxy parameter on cosmological constraints. The shift in the cosmological parameters are shown when a host parameter is added, together with the shift expressed as a fraction of the simple statistical error-bar. A full cosmological analysis is presented in Conley et al. (2010) and Sullivan et al. (2010).

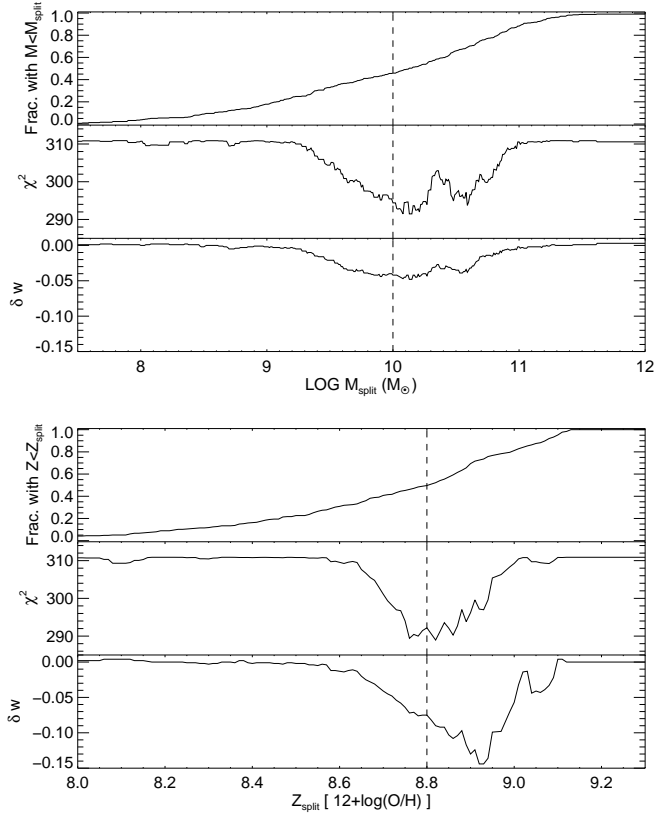


Figure 12. The sensitivity of the cosmological results on the choice of split point used for the host galaxy variable. Cosmological fits are performed at each choice of split point, and the fraction of SNe Ia with the host parameter less than the split point (upper panels), the χ^2 of the fit (middle panels), and the change in w (lower panels) are plotted as a function of the split point. The upper plots show M_{stellar} , the lower ones Z . The default values are shown as vertical lines. The w measures include BAO constraints. When all SNe Ia are assigned to one of the groups as happens on the left and right edges of these plots, the cosmological results are identical. σ_{int} is held fixed in these tests at the values required to produce a reduced χ^2 of one without additional parameters – the decrease in χ^2 can be interpreted as a decrease in σ_{int} when including the host parameter.

in the mix of the two with redshift, will introduce a mild redshift evolution in the mean value of β . Such an evolution has been claimed (Kessler et al. 2009), though is not present to any significant extent in SNLS3 data (Guy et al. 2010). Given the small evolution in M_{stellar} or sSFR with redshift in the SNLS data, we estimate any β evolution would be <0.1 across our entire redshift range, below the detectability of our current dataset.

5.5 Comparison to theory

Timmes et al. (2003) showed that the amount of ^{56}Ni generated in a SN Ia explosion will depend on the metallicity of the progenitor star. More metal-rich stars will generate increased ^{14}N during hydrogen burning as C, N and O are converted to ^{14}N in the CNO cycle. During core helium burning, this ^{14}N is converted to neutron-rich ^{22}Ne , which will favour the production of stable, neutron-rich ^{58}Ni at the expense of the radioactive ^{56}Ni that drives the luminosity of SNe Ia. Fainter SNe Ia should therefore be produced in more metal-rich environments.

While at first sight this may appear to disagree with the results in Figs. 4 and 5 which show the opposite trend, Kasen et al. (2009) show this metallicity effect will also affect the SN light-curve duration – SNe Ia in metal-rich environments are both fainter *and* have narrower light curves (or smaller stretches). Though this trend operates in the same sense as the global stretch–luminosity relation, and is therefore partially corrected by it, the correspondence is not exact and a difference is expected – for a fixed light-curve width, a higher metallicity SN Ia will be brighter. Though the slope of the metallicity-driven stretch–luminosity relation is expected to change with metallicity, over the stretch range that our SNLS data sample (80% of our SNe have $0.9 < s < 1.2$, or $1.2 > \Delta m_{15} > 0.8$ using the relation from Conley et al. (2008)), Kasen et al. (2009) show that the metallicity should act with a fairly constant gradient in stretch–luminosity space. The effect of metallicity should therefore translate to a simple offset in the stretch–luminosity relation derived from our data, rather than a change in slope. This is equivalent to a change in M_B , with brighter SNe in metal-rich environments. Thus this theoretical expectation of progenitor metallicity on SN Ia luminosity appears qualitatively consistent with our data. (Note that these models also predict that SNe Ia in massive galaxies should have slightly smaller stretches due to their high metallicities, all other variables being equal.)

Clearly, other physical variables correlate with host properties such as M_{stellar} and sSFR, including stellar age and dust content (see discussion in Kelly et al. 2009). Dust appears less likely to be responsible for the effects in the SNLS data. The colour–luminosity relations of SNe Ia in low- M_{stellar} and high- M_{stellar} hosts are consistent, as are the mean colours of the SNe in those hosts, as well as the distribution of those colours. There is also the expectation that SNe Ia will be affected by only small amounts of extinction, particularly in flux limited surveys like SNLS (Hatano et al. 1998; Commins 2004).

The role of the progenitor system stellar-age is substantially more complex, and clearly cannot be ruled out in our data – the most massive hosts will on average con-

tain stars of older ages. At the time of writing, no clear prediction has been made as to the effect of progenitor age on SN Ia luminosity. There is speculation that progenitor age drives the global relationship between light-curve shape and host galaxy type, where morphologically earlier-type galaxies host lower-stretch SNe Ia. Of importance in this context is the result that the M_{stellar} –SN-brightness dependency does not depend on the stretch of the SN. Low- s SNe in lower- M_{stellar} hosts have a similar corrected brightness as high- s SNe in low- M_{stellar} hosts, both consistently fainter than their counterparts in high- M_{stellar} hosts. Under the assumption that age is the major driver of the stretch–luminosity relationship, this would suggest that it is metallicity that is responsible for the SN Ia M_{stellar} –luminosity dependence that we observe.

If metallicity is the key physical variable driving the luminosity trends, then the existence of radial metallicity gradients in galaxies (e.g. Henry & Worthey 1999) will complicate the analysis. Studies generally show that the metallicity of galactic disks decreases with increasing galactocentric radius, implying that a simple segregation of SNe based on host galaxy stellar mass or metallicity may (ultimately) require refinement to include, for example, the location of the SN within the host. No trends are apparent between SN residual and galactocentric radius in the SNLS data. However, many factors complicate this analysis, the most pernicious of which is that the measured SN positions must be deprojected (e.g. Ivanov et al. 2000). This requires a knowledge of the structural parameters of the galaxy (for example inclination), difficult to measure for high-redshift galaxies using ground-based data. Additionally, for SNe Ia with long delay times between progenitor formation and explosion, the progenitor star may migrate away from the region in which it is formed. Investigations of this type must await higher-quality low-redshift data.

6 CONCLUSIONS

In this paper we have examined the photometric properties of Type Ia Supernovae (SNe Ia) as a function of their host galaxy properties using new data from the Supernova Legacy Survey (SNLS) and literature data for SNe Ia at low-redshift and $z > 1$. Our principal findings are

- As expected, SN Ia light-curve widths closely track the specific star-formation rate (sSFR) and stellar mass (M_{stellar}) of their host galaxies – massive and/or low sSFR galaxies host SNe Ia with lower stretches (narrower light curves). There is only a mild dependence of SN Ia colour (C) on the host galaxy – SNe Ia in low sSFR galaxies are slightly bluer than those in high-sSFR host galaxies, but the colours of SNe Ia in high- M_{stellar} and low- M_{stellar} hosts are consistent.

- SNe Ia in low sSFR host galaxies, and SNe Ia in massive host galaxies, are systematically brighter by 0.06–0.09 mag ($> 3\sigma$) after light-curve shape and colour corrections. This is not dependent on any assumed cosmological model. Interpreting M_{stellar} as an approximate metallicity indicator, this implies that metal-rich environments host brighter SNe Ia post-correction.

- Galaxies with low sSFRs host SNe Ia with a smaller slope (β) between SN Ia luminosity and colour, and which

have a smaller scatter on Hubble diagrams. This is dependent on the maximum colour of the SN which is considered – the effect is more significant ($2\text{--}3\sigma$) when redder SNe are included. The slope of the relationship between stretch and luminosity is consistent for SNe Ia across different galaxy types.

- The SN Ia luminosity variation with host properties introduces a systematic error into cosmological analyses, as the mean M_{stellar} and sSFR of the hosts, and hence the mix of SNe Ia, evolves with redshift. This effect is exacerbated by the biased selection of existing low-redshift SNe Ia, and amounts to a systematic error on w comparable to the statistical errors.

- We propose that this be corrected for in all future SN Ia cosmological analyses by incorporating a host galaxy term into the fit. Specifically, we show that the use of two absolute magnitudes for SNe Ia, one for those in low- M_{stellar} (or low-metallicity) hosts, and one for events in more massive, metal-rich hosts, leads to an improvement in cosmological fits at $3.8\text{--}4.5\sigma$, and removes the host dependence.

- The SN Ia luminosity effects appear consistent with theoretical expectations of the dependence of SN Ia luminosities on progenitor metallicity. The effect of metallicity is predicted to translate into an offset in the effective stretch–luminosity relation, with brighter SNe in metal-rich environments after correction, as observed in our data.

These results are consistent with earlier observational studies which have found evidence for SN Ia luminosity variation as a function of host galaxy properties at $2\text{--}2.5\sigma$ confidence (Gallagher et al. 2008; Hicken et al. 2009b; Kelly et al. 2009). The SNLS dataset, spanning a larger range in host M_{stellar} and a less biased selection of SNe Ia than at low redshift, provides tighter constraints on host galaxy dependencies and broadly supports the results of these earlier studies.

Redshift evolution in SN Ia properties driven by metallicity effects in the SN Ia population has been suggested as a systematic error in SN Ia cosmology for many years (Höflich et al. 1998, 2000; Domínguez et al. 2001; Timmes et al. 2003; Kasen et al. 2009). The results of this paper detect this evolution, demonstrate that it is qualitatively consistent with theoretical predictions, and show that it can be corrected using supplementary information on the environments in which the SNe explode. There are two key implications from the perspective of measuring dark energy. The first is that additional information on the SN Ia host galaxies, such as multi-colour photometry covering a broad wavelength range, will be an essential requirement for future SN Ia cosmological analyses and surveys. Multi-colour, rolling searches similar to SNLS are obviously well-placed to provide this information as a natural product of the survey strategy.

The second implication is the urgent need for new low-redshift SN Ia samples, where events are selected without regard to their host galaxy type or brightness. Existing searches are mostly galaxy targeted – repeatedly imaging the same catalogued galaxies – and result in heavily biased samples of SNe Ia. The Nearby Supernova Factory (Aldering et al. 2002), and the next generation low-redshift surveys such as the Palomar Transient Factory (PTF; Rau et al. 2009; Law et al. 2009) and SkyMapper

(Keller et al. 2007), should provide samples of SNe Ia selected in a similar way to those at higher redshift, reducing the systematic uncertainties associated with evolving galaxy populations.

ACKNOWLEDGEMENTS

MS acknowledges support from the Royal Society. This paper is based in part on observations obtained with MegaPrime/MegaCam, a joint project of CFHT and CEA/DAPNIA, at the Canada-France-Hawaii Telescope (CFHT) which is operated by the National Research Council (NRC) of Canada, the Institut National des Sciences de l'Univers of the Centre National de la Recherche Scientifique (CNRS) of France, and the University of Hawaii. This work is based in part on data products produced at the Canadian Astronomy Data Centre as part of the CFHT Legacy Survey, a collaborative project of NRC and CNRS. Based in part on observations obtained with WIRCam, a joint project of CFHT, Taiwan, Korea, Canada, France, at the Canada-France-Hawaii Telescope (CFHT) which is operated by the National Research Council (NRC) of Canada, the Institut National des Sciences de l'Univers of the Centre National de la Recherche Scientifique of France, and the University of Hawaii. This work is based in part on data products produced at TERAPIX, the WIRDS (WIRCam Deep Survey) consortium, and the Canadian Astronomy Data Centre. This research was supported by a grant from the Agence Nationale de la Recherche ANR-07-BLAN-0228. Canadian collaboration members acknowledge support from NSERC and CIAR; French collaboration members from CNRS/IN2P3, CNRS/INSU and CEA. Based in part on observations made with ESO Telescopes at the Paranal Observatory under program IDs 171.A-0486 and 176.A-0589. Based in part on observations obtained at the Gemini Observatory, which is operated by the Association of Universities for Research in Astronomy, Inc., under a cooperative agreement with the NSF on behalf of the Gemini partnership: the National Science Foundation (United States), the Science and Technology Facilities Council (United Kingdom), the National Research Council (Canada), CONICYT (Chile), the Australian Research Council (Australia), Ministério da Ciência e Tecnologia (Brazil) and Ministerio de Ciencia, Tecnología e Innovación Productiva (Argentina). The programmes under which data were obtained at the Gemini Observatory are: GS-2003B-Q-8, GN-2003B-Q-9, GS-2004A-Q-11, GN-2004A-Q-19, GS-2004B-Q-31, GN-2004B-Q-16, GS-2005A-Q-11, GN-2005A-11, GS-2005B-Q-6, GN-2005B-Q-7, GN-2006A-Q-7, and GN-2006B-Q-10. Some of the data presented herein were obtained at the W.M. Keck Observatory, which is operated as a scientific partnership among the California Institute of Technology, the University of California and the National Aeronautics and Space Administration. The Observatory was made possible by the generous financial support of the W.M. Keck Foundation. Based on observations made with the NASA/ESA Hubble Space Telescope, obtained at the Space Telescope Science Institute, which is operated by the Association of Universities for Research in Astronomy, Inc., under NASA contract NAS 5-26555.

REFERENCES

- Aldering G., et al., 2002, in *Survey and Other Telescope Technologies and Discoveries*. Edited by Tyson, J. Anthony; Wolff, Sidney. *Proceedings of the SPIE*, Volume 4836, pp. 61-72 (2002)., pp. 61–72
- Astier P., et al., 2006, *A&A*, 447, 31
- Aubourg É., Tojeiro R., Jimenez R., Heavens A., Strauss M. A., Spergel D. N., 2008, *A&A*, 492, 631
- Baldry I. K., Glazebrook K., 2003, *ApJ*, 593, 258
- Balland C., et al., 2009, *A&A*, 507, 85
- Bazin G., et al., 2009, *A&A*, 499, 653
- Bertin E., Arnouts S., 1996, *A&AS*, 117, 393
- Boulade O., et al., 2003, in *Instrument Design and Performance for Optical/Infrared Ground-based Telescopes*. Edited by Iye, Masanori; Moorwood, Alan F. M. *Proceedings of the SPIE*, Volume 4841, pp. 72-81 (2003)., pp. 72–81
- Bronder T. J., et al., 2008, *A&A*, 477, 717
- Buitrago F., Trujillo I., Conselice C. J., Bouwens R. J., Dickinson M., Yan H., 2008, *ApJ*, 687, L61
- Cid Fernandes R., Mateus A., Sodré L., Stasińska G., Gomes J. M., 2005, *MNRAS*, 358, 363
- Comins E. D., 2004, *New Astronomy Review*, 48, 567
- Conley A., Carlberg R. G., Guy J., Howell D. A., Jha S., Riess A. G., Sullivan M., 2007, *ApJ*, 664, L13
- Conley A., et al., 2008, *ApJ*, 681, 482
- Conley A. J., et al., 2010, in prep.
- Contreras C., et al., 2010, *AJ*, 139, 519
- Cooper M. C., Newman J. A., Yan R., 2009, *ApJ*, 704, 687
- Corwin Jr. H. G., Buta R. J., de Vaucouleurs G., 1994, *AJ*, 108, 2128
- Domínguez I., Höflich P., Straniero O., 2001, *ApJ*, 557, 279
- Eisenstein D. J., et al., 2005, *ApJ*, 633, 560
- Ellis R. S., et al., 2008, *ApJ*, 674, 51
- Fioc M., Rocca-Volmerange B., 1997, *A&A*, 326, 950
- Fitzpatrick E. L., Massa D., 2007, *ApJ*, 663, 320
- Folatelli G., et al., 2010, *AJ*, 139, 120
- Gallagher J. S., Garnavich P. M., Berlind P., Challis P., Jha S., Kirshner R. P., 2005, *ApJ*, 634, 210
- Gallagher J. S., Garnavich P. M., Caldwell N., Kirshner R. P., Jha S. W., Li W., Ganeshalingam M., Filippenko A. V., 2008, *ApJ*, 685, 752
- Gallazzi A., Charlot S., Brinchmann J., White S. D. M., Tremonti C. A., 2005, *MNRAS*, 362, 41
- Garnavich P. M., et al., 2004, *ApJ*, 613, 1120
- Giavalisco M., et al., 2004, *ApJ*, 600, L93
- Guy J., et al., 2007, *A&A*, 466, 11
- Guy J., et al., 2010, in prep.
- Guzman R., et al., 1997, *ApJ*, 489, 559
- Höflich P., Nomoto K., Umeda H., Wheeler J. C., 2000, *ApJ*, 528, 590
- Höflich P., Wheeler J. C., Thielemann F. K., 1998, *ApJ*, 495, 617
- Hamuy M., Phillips M. M., Maza J., Suntzeff N. B., Schommer R. A., Aviles R., 1995, *AJ*, 109, 1
- Hamuy M., et al., 1996a, *AJ*, 112, 2408
- Hamuy M., Phillips M. M., Suntzeff N. B., Schommer R. A., Maza J., Aviles R., 1996b, *AJ*, 112, 2398
- Hamuy M., Trager S. C., Pinto P. A., Phillips M. M., Schommer R. A., Ivanov V., Suntzeff N. B., 2000, *AJ*, 120, 1479

- Hatano K., Branch D., Deaton J., 1998, *ApJ*, 502, 177
- Henry R. B. C., Worthey G., 1999, *PASP*, 111, 919
- Hicken M., et al., 2009a, *ApJ*, 700, 331
- Hicken M., et al., 2009b, *ApJ*, 700, 1097
- Howell D. A., et al., 2009, *ApJ*, 691, 661
- Howell D. A., Sullivan M., Conley A., Carlberg R., 2007, *ApJ*, 667, L37
- Howell D. A., et al., 2005, *ApJ*, 634, 1190
- Ivanov V. D., Hamuy M., Pinto P. A., 2000, *ApJ*, 542, 588
- Jha S., et al., 2006, *AJ*, 131, 527
- Jha S., Riess A. G., Kirshner R. P., 2007, *ApJ*, 659, 122
- Kasen D., Röpke F. K., Woosley S. E., 2009, *Nature*, 460, 869
- Keller S. C., et al., 2007, *Publications of the Astronomical Society of Australia*, 24, 1
- Kelly P. L., Hicken M., Burke D. L., Mandel K. S., Kirshner R. P., 2009, *ArXiv e-prints*
- Kessler R., et al., 2009, *ApJS*, 185, 32
- Kewley L. J., Ellison S. L., 2008, *ApJ*, 681, 1183
- Krisciunas K., Prieto J. L., Garnavich P. M., Riley J.-L. G., Rest A., Stubbs C., McMillan R., 2006, *AJ*, 131, 1639
- Lamareille F., et al., 2009, *A&A*, 495, 53
- Landolt A. U., 1992, *AJ*, 104, 340
- Law N. M., et al., 2009, *PASP*, 121, 1395
- Le Borgne D., Rocca-Volmerange B., 2002, *A&A*, 386, 446
- Mannucci F., Della Valle M., Panagia N., 2006, *MNRAS*, 370, 773
- Mannucci F., della Valle M., Panagia N., Cappellaro E., Cresci G., Maiolino R., Petrosian A., Turatto M., 2005, *A&A*, 433, 807
- Neill J. D., Hudson M. J., Conley A., 2007, *ApJ*, 661, L123
- Neill J. D., et al., 2009, *ApJ*, 707, 1449
- Nobili S., Goobar A., 2008, *A&A*, 487, 19
- Perlmutter S., et al., 1999, *ApJ*, 517, 565
- Perrett K. J., et al., 2010, in *AJ*, submitted
- Phillips M. M., 1993, *ApJ*, 413, L105
- Phillips M. M., Lira P., Suntzeff N. B., Schommer R. A., Hamuy M., Maza J. ., 1999, *AJ*, 118, 1766
- Pozzetti L., et al., 2007, *A&A*, 474, 443
- Pritchett C. J., Howell D. A., Sullivan M., 2008, *ApJ*, 683, L25
- Rana N. C., Basu S., 1992, *A&A*, 265, 499
- Raskin C., Scannapieco E., Rhoads J., Della Valle M., 2009, *ApJ*, 707, 74
- Rau A., et al., 2009, *PASP*, 121, 1334
- Regnault N., et al., 2009, *A&A*, 506, 999
- Retzlaff J., Rosati P., Dickinson M., Vandame B., Rite C., Nonino M., Cesarsky C., the GOODS Team, 2010, *A&A*, 511, 50
- Riess A. G., et al., 1999, *AJ*, 117, 707
- Riess A. G., Press W. H., Kirshner R. P., 1996, *ApJ*, 473, 88
- Riess A. G., et al., 2004, *ApJ*, 607, 665
- Riess A. G., et al., 2007, *ApJ*, 659, 98
- Salpeter E. E., 1955, *ApJ*, 121, 161
- Sarkar D., Amblard A., Cooray A., Holz D. E., 2008, *ApJ*, 684, L13
- Savaglio S., et al., 2005, *ApJ*, 635, 260
- Savaglio S., Glazebrook K., LeBorgne D., 2009, *ApJ*, 691, 182
- Scannapieco E., Bildsten L., 2005, *ApJ*, 629, L85
- Schawinski K., 2009, *MNRAS*, 397, 717
- Sullivan M., et al., 2003, *MNRAS*, 340, 1057
- Sullivan M., Ellis R. S., Howell D. A., Riess A., Nugent P. E., Gal-Yam A., 2009, *ApJ*, 693, L76
- Sullivan M., et al., 2006, *ApJ*, 648, 868
- Sullivan M., et al., 2010, in prep.
- Takanashi N., Doi M., Yasuda N., 2008, *MNRAS*, 389, 1577
- Timmes F. X., Brown E. F., Truran J. W., 2003, *ApJ*, 590, L83
- Totani T., Morokuma T., Oda T., Doi M., Yasuda N., 2008, *PASJ*, 60, 1327
- Tremonti C. A., et al., 2004, *ApJ*, 613, 898
- Tripp R., 1998, *A&A*, 331, 815
- Wang L., 2005, *ApJ*, 635, L33
- Williams B. F., et al., 2003, *AJ*, 126, 2608